Center for Aeronautical Research

Bureau of Engineering Research
The University of Texas at Austin
Austin, Texas

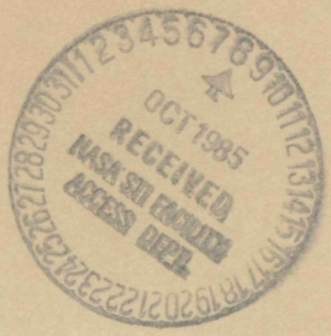

CAR 85-1

SUBSTRUCTURE COUPLING
IN THE
FREQUENCY DOMAIN

Randall C. Bachmeyer
Roy R. Craig, Jr.

NASA Contract No. NAS8-35338

May, 1985

SUBSTRUCTURE COUPLING IN THE FREQUENCY DOMAIN

A Report to

NASA Marshall Space Flight Center

Contract No. NAS8-35338

by

Randall C. Bachmeyer *

Roy R. Craig, Jr. +

ASE-EM Department

The University of Texas at Austin

Austin, Texas 78712

* Graduate Student

+ Professor, ASE-EM
Prinicipal Investigator

May 1985

TABLE OF CONTENTS

ACKNOWLEDGMENTS

This work was supported by Contract NAS8-35338 of the NASA George C. Marshall Space Flight Center. The authors wish to thank Mr. Larry Kiefling for his interest in this work.

Chapter 1

INTRODUCTION

1.1 Structural Dynamics

Today, every airplane, booster, and spacecraft in production has been subjected to a very thorough dynamic analysis. However, it is not only the aerospace industry that is interested in structural dynamics. The interest has spread through a range of industries which manufacture everything from automobiles to typewriters, and construction companies which build everything from bridges to high-rise office buildings.

The reason for wanting a dynamic analysis may vary from company to company, but certain requirements of the analysis remain constant. It must be accurate, it must be low cost, and it must be completed quickly. Today's structural dynamicists are addressing each of these requirements.

One of the most popular approaches to satisfying these requirements involves the use of substructures.

1.2 Reasons for Substructuring

Structural systems have become so complex today that no single engineer, and often no single company, is capable of efficiently designing and analyzing the entire structure alone. The structures are too large and too complex to handle on the system level, and are therefore broken down into smaller structures (i.e. substructures). The three primary reasons for substructuring are:

1. Different groups or companies specialize in one particular part of a structure, and are the most qualified to design that part. Therefore the structure is separated into substructures, and each substructure is given to the group which specializes in its design.

2. When a single group or company is given responsibility for the entire structure, the project is often more easily managed if the structure is separated into substructures. Each substructure may then be designed and verified independently before assembling all the substructures to verify the superstructure.

3. From a computational point of view, it is often the case that a coupled substructure analysis will yield a more efficient analysis of the structure than will a single analysis of the entire structure.

Having discussed the reasons for substructuring, the actual dynamic analysis will now be considered. General analysis techniques will be discussed first, and substructure analysis techniques will be discussed subsequently.

1.3 Current Response Analyses

The dynamic analysis of a structure may include several analyses including a modal analysis, a shock spectrum analysis, or a response analysis to a particular dynamic load. The primary focus of this paper will be on the latter.

Currently, there are two basic types of analyses used to obtain the system response to dynamic load. They may be classified as (1) time-domain analyses, and (2) frequency-domain analyses.

Time-domain analysis techniques commonly attempt to uncouple the system equations and then integrate them directly. This uncoupling of the equations of motion is accomplished by using a modal transformation. Since the transformation matrix must be orthogonal with respect to the mass, stiffness, and damping matrices, it is often found by solving the eigenvalue problem which arises from the free vibration problem and subsequently assuming a form of damping which leaves the modes uncoupled.

Frequency-domain analysis techniques use either Laplace or Fourier transformations to transform the differential equations of motion to the frequency domain, where they become algebraic equations. The system of linear algebraic equations may then be solved for the system response. This frequency-domain response may then be inverse transformed to obtain the response in the time domain.

1.4 Substructure Coupling in the Frequency Domain

When utilizing a frequency-domain procedure for coupling substructures, only the dynamic stiffness matrices for each substructure are required. The system equations are then obtained by using a direct stiffness approach to couple the substructure dynamic stiffness matrices. This set of linear equations may then be solved for the system response.

There are some instances where the frequency-domain techniques are more efficient than time-domain techniques. However, there are some instances where this is reversed. Since each of these methods is capable of giving either exact or approximate solutions, this paper will frequently compare the efficiency of the two procedures, and consequently will often discuss the cost of a particular operation. This cost is most accurately defined as the amount of standardized computer time required for that particular operation.

1.5 Current Frequency Domain Analysis

The best-known frequency-domain analysis is the harmonic or steady-state analysis. This frequency-domain technique has been used for many years to determine the steady-state response of structures subjected to periodic loads, and has been implemented in several of the large general purpose finite element packages (Ref. 1, 2). An equally well-known frequency-domain analysis is the determination of the spectral response of a structure to random loads (Ref. 3, 4).

Little work has been done in the area of determining the transient response of structures using frequency-domain techniques. It is surmised that this is because of the problems encountered when transforming problems between the discrete time and frequency domains, and because of the expense of frequency-domain analysis of a large unreduced system. Each of these topics will be addressed in subsequent chapters of this thesis.

An area of frequency-domain analysts which is becoming popular among analysts is the representation of substructures by frequency-

dependent matrices. These methods are often denoted as impedance methods, and various papers have been published on the topic by Chopra, Poelart, Payne, Geering, and Williams and Wittrick (Ref. 3, 5, 6, 7, 8).

Chopra uses frequency-domain methods to perform earthquake analyses of concrete dams. He uses frequency-domain representations of the soil and the dam which are derived from finite element models to obtain his system equations of motion. He reduces the number of degrees of freedom through the use of Ritz vectors.

Poelart presents a distributed-element approach to the frequency-domain method, where an element is represented by its exact impedance matrix. His paper also presents a discussion of the problems associated with using finite elements in a dynamic analysis, as he compares the distributed element approach to the finite element approach.

The paper by Payne presents an approach by which two finite element substructure models may be coupled using the impedance matrix of each substructure. He uses modal expansions of each substructure to determine the respective impedance matrices. His paper gives particular emphasis to problems with statically-determinate interfaces. Payne also provides for a reduction in the computational effort when structural modifications are performed on one of the substructures.

The work by Geering is primarily concerned with the coupling of substructures represented by frequency-dependent matrices, and the reduction in the number of degrees of freedom required for an analysis.

Each of these topics is discussed in subsequent chapters, as much of this paper is based on the work of Geering.

The computation of natural frequencies using frequency-domain techniques has been investigated by Williams and Wittrick. In their work, each of the elements of a structure is represented by its dynamic stiffness matrix. Their procedure for determining natural frequencies is discussed in subsequent chapters also.

Using these papers to establish the current state of the art in frequency-domain analysis, the research goals for this thesis were then determined.

1.6 Research Goals

The primary goal of this research project was to obtain a clear understanding of the strengths and weaknesses of substructure coupling in the frequency domain. These qualities were then to be evaluated and used to determine where the method is particularly applicable, and where it is not.

The secondary goal was to determine the generality of the method. This was to be accomplished by determining if a substructured model which had been created in the frequency domain could be used to obtain the system natural frequencies.

It is not the purpose of the research project to demonstrate new analytical techniques, although some have been presented. The purpose of the paper is to provide an analyst with sufficient information about the strengths and weaknesses of substructure coupling in the frequency domain. The analyst should then be able to make a decision

regarding the usefulness of the method for a particular application. An attempt has also been made to provide sufficient detail to permit implementation of the Geering method if so desired.

1.7 Organization of the Thesis

This thesis has been organized into eight chapters. The first chapter provides justification and background for the work presented in subsequent chapters.

Chapter 2 describes the system equations of motion, and the analytical tools necessary to transform the equations to the frequency domain. The chapter discusses both steady state and transient analysis. Chapter 3 proceeds with a discussion of the implementation of frequency-domain analysis on a digital computer, and Chapter 4 discusses Geering's method of coupling substructures in the frequency domain (Ref. 3). Chapters 2, 3 and 4 are included as support for the primary research goal.

The support for the secondary research goal is included in Chapters 5 and 6, which outline procedures which may be used to determine the natural frequencies of undamped and damped structures respectively. Chapter 5 is based on work by Williams and Wittrick (Ref. 6) in their search for natural frequencies of continuous systems, while Chapter 6 presents some original work on determining the natural frequencies of damped systems.

Chapter 7 presents examples to support the equations of Chapters 2 through 6, and Chapter 8 is the final chapter which includes

some general comments on substructure coupling in the frequency domain. Directions for further research are also presented in Chapter 8.

Chapter 2

FREQUENCY-DOMAIN ANALYSIS

2.1 Equations of Motion

Consider a finite element model of a structure with n active degrees of freedom.[1] The model may be formed using either lumped mass matrices or consistent mass matrices. The damping may be proportional, nonproportional, hysteretic, or any other linear form. In other words, the analyst is free to model the structure in various ways, as long as the equations of motion for the system may be written as

$$[m]\{\ddot{x}(t)\} + [c]\{\dot{x}(t)\} + [k]\{x(t)\} = \{f(t)\} \qquad (2.1)$$

[m], [c], and [k] are time-invariant matrices commonly denoted as the mass, damping, and stiffness matrices respectively. The $\{\ddot{x}(t)\}$, $\{\dot{x}(t)\}$, and $\{x(t)\}$ vectors represent the acceleration, velocity, and displacement of each of the n degrees of freedom. Likewise, the $\{f(t)\}$ vector represents the load applied at each of the n degrees of freedom. The initial displacement and initial velocity vectors will be written as

$$\{x(t=0)\} = \{x_0\} \qquad (2.2a)$$

and

$$\{\dot{x}(t=0)\} = \{\dot{x}_0\} \qquad (2.2b)$$

---

[1] Equations throughout this thesis will include only active degrees of freedom, which are those degrees of freedom which have not been constrained to have zero displacement.

Equation (2.1) represents a system of n linear second order differential equations. However, by applying carefully selected transformations, the equations may be transformed into a system of n linear algebraic equations.

This chapter will examine three such transform pairs which allow the equations to be transformed to the new domain, and the solution to be inverse transformed back to the time domain. Each transformation will be examined to determine (1) whether it gives a steady state or transient solution, (2) whether there are restrictions on the type of excitation, and (3) whether the system is permitted to be damped or undamped.

2.2 Fourier Integral Transforms

The Fourier integral transform is one of the most popular transformations because of the ease with which it may be discretized and implemented on a digital computer. The unilateral Fourier integral transform will be used in this paper, since all excitation and responses will be assumed to be identically zero before some instant in time (t=0 for this paper).

Given a general function $y(t)$, the unilateral Fourier integral transform pair may be written

$$Y(\omega) = \int_0^\infty y(t)\, e^{-j\omega t}\, dt \qquad (2.3a)$$

$$y(t) = \frac{1}{2\pi} \int_{-\infty}^{\infty} Y(\omega) e^{j\omega t}\, d\omega \qquad (2.3b)$$

where ω is a real variable, often denoted as the frequency variable.

The equation of motion in the frequency domain may be obtained by applying the transformation given by Eq. (2.3a) to Eq. (2.1). Appendix A.1 gives the details of the transformation which yields

$$\begin{aligned}&\left[-\omega^2\,[m] + j\omega\,[c] + [k]\right]\{X(\omega)\}\\ &= \{\tilde{F}(\omega)\} + [m]\,\{\dot{x}_0\} + \left[j\omega\,[m] + [c]\right]\{x_0\}\end{aligned} \tag{2.4}$$

or in shorthand notation,

$$[G(\omega)]\,\{X(\omega)\} = \{F(\omega)\} \tag{2.5}$$

where the dynamic stiffness matrix, $[G(\omega)]$, is given by

$$[G(\omega)] = -\omega^2\,[m] + j\omega\,[c] + [k] \tag{2.6}$$

and

$$[F(\omega)] = \{\tilde{F}(\omega)\} + [m]\,\{\dot{x}_0\} + \left[j\omega\,[m] + [c]\right]\{x_0\} \tag{2.7}$$

where $\{\tilde{F}(\omega)\}$ is the unilateral Fourier integral transform of the forcing function $\{f(t)\}$, and $\{x_0\}$ and $\{\dot{x}_0\}$ are the initial displacement and velocity vectors respectively.

The response spectrum may then be obtained by solving the system of linear equations in Eq. (2.5). Thus,

$$\{X(\omega)\} = [H(\omega)]\,\{F(\omega)\} \tag{2.8}$$

where the dynamic flexibility matrix, $[H(\omega)]$, is given by

$$[H(\omega)] = [G(\omega)]^{-1} \tag{2.9}$$

The time-domain response may then be obtained by inverse transforming $\{X(\omega)\}$ using Eq. (2.3b).

Careful consideration must be given to the restrictions and assumptions made in Appendix A.1, as they determine the class of problems which may be solved using the Fourier integral transform approach. In short, they may be stated:

- The forcing function $\{f(t)\}$ must be of finite duration, and therefore nonperiodic.
- The system must be damped.

If these conditions are satisfied, the inverse transform of the spectrum given by Eq. (2.8) will yield the exact, or as it is often called, the transient solution to Eq. (2.1).

In summary, the unilateral Fourier integral transform approach may be used to solve for the transient response of damped systems subjected to finite duration excitation.

2.3 Fourier Integral Transforms with Convergence Functions

An investigation of the Fourier transformability conditions in Appendix A.1 reveals that the class of problems which may be worked using the Fourier integral transform approach is limited because of the condition that the integral,

$$\int_0^\infty |y(t)|\, dt \tag{2.10}$$

must converge. This convergence condition necessitated the restriction of finite-duration excitation and response.

Therefore, in order that the Fourier integral transform approach may be used for systems not satisfying the convergence condition, Eq. (2.1) will be multiplied by a yet unknown function, $b(t)$,

$$b(t)\left[[m]\{\ddot{x}\} + [c]\{\dot{x}\} + [k]\{x\}\right] = b(t)\{f(t)\} \qquad (2.11)$$

where $b(t)$ is any function which will cause Eq. (2.11) to satisfy the convergence conditions when transformed. The unilateral Fourier integral transform may now be applied to Eq. (2.11) and written

$$\int_0^\infty b(t)\left[[m]\{\ddot{x}\} + [c]\{\dot{x}\} + [k]\{x\}\right] e^{-j\omega t}\, dt = \qquad (2.12)$$

$$\int_0^\infty b(t)\ \{f(t)\}\ e^{-j\omega t}\, dt$$

Now assume that the convergence function, $b(t)$, is given by

$$b(t) = e^{-at} \qquad (2.13)$$

where the convergence factor, a , is any value which will cause Eq. (2.11) to satisfy the convergence conditions when transformed.

Equation (2.13) may now be substituted into equation (2.12) to yield

$$\int_0^\infty \left[[m]\{\ddot{x}\} + [c]\{\dot{x}\} + [k]\{x\}\right] e^{-at}\ e^{-j\omega t}\, dt = \qquad (2.14)$$

$$\int_0^\infty \{f(t)\}\ e^{-at}\, e^{-j\omega t}\, dt$$

An examination of the transformability of Eq. (2.14) reveals that the integrals

$$\int_0^\infty \left[[m]\{\ddot{x}\} + [c]\{\dot{x}\} + [k]\{x\}\right] e^{-at}\, dt \tag{2.15}$$

and

$$\int_0^\infty \{f(t)\}\, e^{-at}\, dt \tag{2.16}$$

must converge. It has been shown that for forcing functions of exponential order α_0, (i.e. for those functions which have the property that there is a real number, α_0, such that

$$\lim_{t\to\infty} \{f(t)\}\, e^{-\alpha t} = 0 \quad \text{when} \quad \alpha > \alpha_0 \tag{2.17}$$

and with the limit not existing when $\alpha < \alpha_0$;) Eq. (2.16) will converge for $a > \alpha_0$. (Ref. 9). It has also been shown that since the response of stable linear systems is at least of exponential order 0, Eq. (2.15) will always converge for $a > 0$, and will converge for $a \leq 0$ when the system and excitation is of the type described in Section 2.2.

In light of these guarantees for convergence, the restrictions which required the excitation and response to be of finite duration may be lifted. It is interesting to note, however, that the selection of a 'large' convergence factor will cause the integrands of Eq. (2.12) to approach zero 'very fast,' simulating a finite duration excitation and response.

Equation (2.14) may now be simplified and written

$$\int_0^\infty \left[[m]\{\ddot{x}\} + [c]\{\dot{x}\} + [k]\{x\}\right] e^{-st}\, dt = \int_0^\infty \{f(t)\}\, e^{-st}\, dt \tag{2.18}$$

where the complex frequency variable, s, is given by

$$s = a + j\omega \tag{2.19}$$

At this point, Eq. (2.18) may be integrated by parts as detailed in Appendix A.2, and written

$$\left[[m]s^2 + [c]s + [k]\right]\{X(s)\} = \{\tilde{F}(s)\} + [m]\{\dot{x}_0\} + \left[[m]s + [c]\right]\{x_0\} \tag{2.20}$$

or in shorthand notation as

$$[G(s)]\{X(s)\} = \{F(s)\} \tag{2.21}$$

where

$$[G(s)] = [m]s^2 + [c]s + [k] \tag{2.22}$$

and

$$\{F(s)\} = \{\tilde{F}(s)\} + [m]\{\dot{x}_0\} + \left[[m]s + [c]\right]\{x_0\} \tag{2.23}$$

It has been shown in Appendix A.2 that

$$\tilde{F}(s) = \int_0^\infty f(t) \quad e^{-st} \quad dt \tag{2.24}$$

or

$$\tilde{F}(s) = \int_0^\infty f(t) \quad e^{-at} \quad e^{-j\omega t} \quad dt \tag{2.25}$$

which is simply the unilateral Fourier integral transform of $\{\hat{f}(t)\}$, where

$$\{\hat{f}(t)\} = \{f(t)\} \quad e^{-at} \tag{2.26}$$

As in the previous section, Eq. (2.1) may be solved for $\{X(s)\}$, yielding

$$\{X(s)\} = [H(s)] \{F(s)\} \tag{2.27}$$

where

$$[H(s)] = [G(s)]^{-1} \tag{2.28}$$

Referencing Appendix A.2 once again, reveals that

$$\{X(s)\} = \int_0^\infty \{x\} \quad e^{-st} \quad dt \tag{2.29}$$

or

$$\{X(s)\} = \int_0^\infty \{x\} \quad \bar{e}^{at} \quad \bar{e}^{j\omega t} \quad dt \tag{2.30}$$

which is simply the unilateral Fourier integral transform of $\{\hat{x}\}$, where

$$\{\hat{x}\} = \{x\}\ e^{-at} \tag{2.31}$$

Therefore, the inverse unilateral Fourier integral transform of $\{X(s)\}$ does not yield $\{x\}$, but instead yields $\{\hat{x}\}$. However, $\{x\}$ may be recovered using the relationship

$$\{x\} = \{\hat{x}\}\ e^{at} \tag{2.32}$$

At this point, it should be clear that when the convergence function, e^{-at}, is used in conjunction with the unilateral Fourier integral transformation, the transform is equivalent to the Laplace transformation, where the complex frequency variable, s, is simply the Laplace variable. The detailed discussion of the convergence function was undertaken in this section, (1) to emphasize why the Laplace transform removes some of the restrictions of the Fourier transform, (2) to emphasize that unilateral Fourier integral transformations may be used to perform forward and inverse Laplace transforms once a convergence factor has been selected, and (3) to give some physical insight into what exactly the convergence function does, in order to aid in the selection of the convergence factor.

Therefore, the unilateral Fourier integral transformation, used in conjunction with a convergence function, e^{-at}, may be used to solve for the transient response of a damped or undamped system subjected to any excitation of exponential order.

2.4 Complex Fourier Series

In the previous sections, methods of obtaining the transient response of a system were discussed. However, there are instances when only the steady-state response to a periodic excitation is desired.

For this class of problems, the equations of motion may be transformed to the frequency domain using the complex Fourier series transform pair,

$$y(t) = \frac{1}{T_1} \sum_{k=-\infty}^{\infty} Y(\omega_k) \; e^{j\omega_k t} \tag{2.33}$$

$$Y(\omega_k) = \int_{\tau}^{\tau+T_1} y(t) \; e^{-j\omega_k t} \; dt \tag{2.34}$$

where

$$\omega_k = k \left(\frac{2\pi}{T_1} \right) \tag{2.35}$$

and T_1 is the fundamental period of $y(t)$.

The details of the transformation are presented in Appendix A.3. The frequency domain equations of motion are

$$\left[-\omega_k^2 \, [m] + j\omega_k \, [c] + [k] \right] \{X(\omega_k)\} = \{\tilde{F}(\omega_k)\} \tag{2.36}$$

$$k = -\infty, \ldots, \infty$$

where $\{\tilde{F}(\omega_k)\}$ is the forcing spectrum determined by a complex Fourier analysis of $\{f(t)\}$. As in the previous sections, Eq. (2.36) may be simplified and solved for $\{X(\omega_k)\}$

$$[G(\omega_k)]\ \{X(\omega_k)\} = \{\tilde{F}(\omega_k)\} \qquad k = -\infty,\ldots,\infty \qquad (2.37)$$

$$\{X(\omega_k)\} = [H(\omega_k)]\ \{\tilde{F}(\omega_k)\} \qquad k = -\infty,\ldots,\infty \qquad (2.38)$$

where

$$[H(\omega_k)] = [G(\omega_k)]^{-1} \qquad k = -\infty,\ldots,\infty \qquad (2.39)$$

The time-domain response may then be obtained using the inverse transform relation given in Eq. (2.33).

An examination of the transformation detailed in Appendix A.3 will reveal that the time-domain solution obtained is only a particular, or steady-state, solution to the equations of motion given by Eq. (2.1).

Therefore, Chapter 2 has presented two transformations which may be used to obtain the transient response to a limited class of problems. The chapter has also presented a well-known method of obtaining the steady-state response of a system. Now, Chapter 3 will investigate the computational considerations in the implementation of these procedures.

Chapter 3

COMPUTATIONAL CONSIDERATIONS

3.1 Discretizing the Problem

In Chapter 2, three different sets of frequency domain equations of motion were presented. Those presented in Eqs. (2.4) and (2.20) were functions of the continuous variables ω and s respectively, and the equations of motion presented in Eq. (2.36) were functions of the discrete variable ω_k. It is the purpose of this section to consolidate the three sets of equations into one set of discretized equations to be used in the discussion of the frequency-domain computational model.

The first step in the consolidation is to recognize that Eq. (2.4) is identical to Eq. (2.20) when the convergence factor is identically zero. Therefore, since Eq. (2.4) is contained within Eq. (2.20), the latter equation will be used henceforth.

It has been shown by several authors, that the Fourier integral transform and the inverse Fourier integral transform, such as those required in the evaluation of Eq. (2.20), may be approximated by the discrete Fourier transform (DFT) pair (Ref. 4, 10, 11).

Therefore, the discretization of Eq. (2.20) will begin by using the DFT to evaluate $\{\tilde{F}(s)\}$ at k discrete frequencies. The transformation and the resulting force spectrum may be written as

$$(\{\tilde{F}_k\} \;;\; k=0,\ldots,K-1) \equiv \text{DFT}\,(\{f(t)\}^{*}\, e^{-at}) \qquad (3.1)$$

where $\{\tilde{F}_k\}$ is equivalent to $\{\tilde{F}(s_k)\}$. The $\{\ \}^*$ notation indicates that only discrete values of $\{f(t)\}$ are used as required by the DFT algorithm.

Since the force spectrum, as given by Eq. (3.1), is only defined at K discrete frequencies, Eq. (2.20) may only be evaluated at those K frequencies. Thus

$$\begin{aligned}\left[[m]\, s_k^2 + [c]\, s_k + [k]\right] \{X_k\} \\ = \{\tilde{F}_k\} + [m]\, \{\dot{x}_o\} + \left[[m]\, s_k + [c]\right] \{x_o\} \\ k=0,\ldots,K-1\end{aligned} \tag{3.2}$$

Equation (3.2) represents K sets of simultaneous equations which must be solved in order to obtain the discrete response spectrum $(\{X_k\}\ ;\ k=0,\ldots,K-1)$.

This discrete response spectrum may then be inverse transformed to obtain the discrete function, $\{x(t)\}^*\, e^{-at}$, and Eq. (2.31) may be used to determine $\{x(t)\}^*$. Thus,

$$\{x(t)\}^* = e^{at}\, [\text{IDFT}\ (\{X_k\}\ ;\ k=0,\ldots,K-1)] \tag{3.3}$$

where the $\{\ \}^*$ notation again represents a discrete time function.

Having discretized Eq. (2.20), the consolidation of Eqs. (3.2) and (2.36) into a single set of equations will continue. The next step in the consolidation is to recognize the fact that functions of the variable ω_k may be represented as functions of s_k with a

convergence factor of zero. Equation (2.36) may therefore be written as

$$\left[[m]\, s_k^2 + [c]\, s_k + [k]\right] \{X_k\} = \{\tilde{F}_k\} \qquad k=-\infty,\ldots,\infty \tag{3.4}$$

Since it has been shown that the DFT may also be used to approximate the complex Fourier series (Ref. 4), the transformation of the periodic forcing function $\{f(t)\}$ may be written as

$$(\{\tilde{F}_k\} \;;\; k=0,\ldots,K-1) \equiv \text{DFT}\,(\{f(t)\}^*) \tag{3.5}$$

which is equivalent to Eq. (3.1) when the convergence factor is zero.

Again, since the force spectrum is only defined at K discrete frequencies, Eq. (3.4) may only be evaluated at those frequencies. Thus,

$$\left[[m]\, s_k^2 + [c]\, s_k + [k]\right] \{X_k\} = \{\tilde{F}_k\} \qquad k=0,\ldots K-1 \tag{3.6}$$

Now, Eqs. (3.2) and (3.6) may both be written in shorthand notation as

$$[G_k]\, \{X_k\} = \{F_k\} \qquad k=0,\ldots,K-1 \tag{3.7}$$

where

$$[G_k] = [m]\, s_k^2 + [c]\, s_k + [k] \qquad k=0,\ldots,K-1 \tag{3.8}$$

$$\{F_k\} = \{\tilde{F}_k\} + [m]\, \{\dot{x}_0\} + \left[[m]\, s_k + [c]\right] \{x_0\} \qquad k=0,\ldots,K-1 \tag{3.9}$$

and

$$(\{\tilde{F}_k\} \;;\; k=0,\ldots,K-1) \equiv \text{DFT}\,(\{f(t)\}^* e^{-at}) \qquad (3.10)$$

The frequency-domain response spectrum may be found using the relationships

$$\{X_k\} = [H_k]\,\{F_k\} \qquad k=0,\ldots,K-1 \qquad (3.11)$$

where

$$[H_k] = [G_k]^{-1} \qquad k=0,\ldots,K-1 \qquad (3.12)$$

and finally, the time-domain response may be found at discrete values of t from

$$\{x(t)\}^* = e^{at}\,[\text{IDFT}\,(\{X_k\} \;;\; k=0,\ldots,K-1)] \qquad (3.13)$$

Subject to the following modifications, Eqs. (3.7) through (3.13) represent the single computational model which may be implemented to obtain the response of the systems described in Sections 2.2, 2.3, and 2.4.

- To determine the transient response of damped systems to finite duration excitation
  - Set $a \equiv 0$
- To determine the transient response of either damped or undamped systems
  - Select a proper value for the convergence factor (Ref. Section 3.3)

- To determine the steady-state response of either damped or undamped systems to a period input

  - Set $a \equiv 0$

  - Set $\{x_0\} = \{\dot{x}_0\} \equiv \{0\}$ (This is simply a method of getting the algorithm to ignore the initial conditions, since they are not used in steady-state analysis).

Therefore, the solution procedures have been consolidated into a single set of equations which is easily adapted for each desired response analysis. In an attempt to ease the burden of notation in the remainder of this paper, Eqs. (3.7) and (3.11) will be written as

$$[G]\{X\} = \{F\} \tag{3.14}$$

and

$$\{X\} = [H]\{F\} \tag{3.15}$$

where their discreteness is implicit.

The next section will discuss the inherent problems in using the DFT to approximate the Fourier integral transform and the complex Fourier series.

3.2 The Discrete Fourier Transform

When the DFT was introduced in the previous section, it was said to approximate the Fourier integral transform and the complex Fourier series. The interested reader not familiar with the derivation of the DFT and the nature of the approximations made is referred to several books which have been written on the subject (Ref. 10, 4). The

discussion of the DFT included in this paper will be limited to the selection of sampling parameters which will avoid frequency and time-domain aliasing.

When utilizing the DFT, there are many sampling parameters which may be varied, including the sampling frequency, Nyquist frequency, frequency resolution, length of the time record, time resolution, and the number of digital samples. However, using the relationships given in Appendix B, the specification of any two of these parameters will uniquely define the remaining parameters. Therefore, the two parameters will be chosen such that aliasing does not occur.

In order to avoid frequency-domain aliasing, the Nyquist frequency is selected in accordance with the following guidelines:

- For band-limited functions - Select f_N such that it is greater than or equal to the highest frequency contained in the exponentially-windowed forcing function.

- For functions whose spectrum is not band limited - Examine a typical system transfer function and determine the frequency, f_c, where the function effectively decays to zero, (i.e. $H(f>f_c) = 0$). Since $\{X(f>f_c)\} = \{0\}$ in accordance with Eq. (3.15), a value for f_N is then selected such that the exponentially-windowed force spectrum below f_c is represented accurately. Example 1 in Chapter 7 demonstrates this procedure.

Once the Nyquist frequency has been determined, the resolution in the time domain may then be found from

$$T_{max} = \frac{1}{2f_N} \tag{3.16}$$

The time resolution is denoted as a maximum resolution since it may be desired to select a smaller value of T in order that the system response may be obtained with a greater resolution.

Now, in order to avoid time-domain aliasing, the length of the time record, T_o, will be chosen such that both the exponentially-windowed excitation, $\{\hat{F}(t)\}$, and exponentially-windowed response, $\{\hat{x}\}$, have 'effectively decayed to zero' before the end of the time record. The author has found that time-domain aliasing will not be significant if 'effectively zero' is said to mean that the response at the end of the time record is at least two orders of magnitude less than the response at the beginning of the time record.

The remaining sampling parameters may now be determined by using the equations in Appendix B in conjunction with the values of f_N and T_o selected to prevent aliasing. The most important of these parameters is the number of digital samples, K, since it was seen in Eq. (3.2) that the value of K determines how many sets of frequency-domain equations must be solved. Thus, the minimum value of K may be determined from

$$K_{min} = 2T_o f_N \tag{3.17}$$

Once a suitable integer value of K has been chosen, either T_o or f_N must be recalculated since only two parameters may be independently specified.

The DFT is often implemented on the digital computer using the Fast Fourier Transform (FFT) algorithm (Ref. 10, 12) which has a higher computational efficiency than the DFT algorithm. Therefore, the following chapters will use DFT and FFT synonymously, since they differ only in implementation.

It must be noted, however, that in a radix-2 implementation of the FFT, K is required to be an integer power of two. Therefore, if the minimum value of K was determined to be 550, it would be necessary to use a K of 1024. For problems where n is 'large', the cost of the solution of 474 extra sets of equations may be greater than the savings achieved by using the FFT algorithm.

Before performing a DFT on a periodic signal, one additional topic requires discussion. That topic is leakage. In order to prevent leakage, there must be an integer number of fundamental periods of the signal within the time record. This condition can be difficult to satisfy if one is trying to keep f_N and T_o within a certain range to obtain a suitable value of K. A windowing function such as the Hanning or Tukey window may be applied to the function in an attempt to reduce leakage (Ref. 4, 10).

In summary, the selection of the sampling parameters is very important when using the DFT. The following section will discuss the selection of the convergence factor and its influence on the problem of time-domain aliasing.

3.3 The Selection of a Convergence Factor

To prevent time-domain aliasing it is required that both $\{\hat{f}(t)\}$ and $\{\hat{x}\}$ decay to 'effectively zero' by the end of the time record, or window as it is often called. In the previous section it was noted that T_o could be chosen such that this criterion would be satisfied for any value of a. However, it is often more efficient to chose T_o to be the maximum time at which the response is desired. Since this value of T_o is often less than the T_o required to prevent time-domain aliasing for an arbitrary a, the value of K_{min} will be reduced in accordance with Eq. (3.17).

Therefore, if T_o is selected without regard for the aliasing problem, the value of the convergence factor must be selected such that the functions $\{\hat{f}(t)\}$ and $\{\hat{x}\}$ decay to 'effectively zero' by the end of the window. An examination of Eqs. (2.26) and (2.31) reveals that an increased value of the convergence factor will cause the functions to decay faster and will further reduce the chances of time-domain aliasing. Therefore, it appears that the convergence factor should be chosen to be 'very large.'

Although there is no limit on the maximum value of the convergence factor from an analytical standpoint, there is a limit imposed from a computational standpoint. The problem occurs when large values of a are used such that the order of magnitude of the functions at opposite ends of the window are vastly different. This large variation in magnitude causes the computational model to be ill-conditioned in a finite word length computer, and therefore causes roundoff errors.

In a limited number of tests, this author concluded that the convergence function should not cause the original function to change more than two or three orders of magnitude within the window. A good rule of thumb for the maximum value of the convergence factor was found to be

$$a_{max} = \frac{-\ell n(10^{-2}/e^{\alpha_o T_o})}{T_o} \qquad (3.18)$$

where α_o is the exponential order of the forcing function. This convergence factor causes the function to change two orders of magnitude within the window.

In summary, the value of the convergence factor must be greater than zero as determined in Chapter 2, and it must be large enough to prevent time-domain aliasing, while remaining small enough to prevent ill-conditioning of the computational model.

This concludes the discussion of parameter selection to obtain an efficient and well-conditioned frequency-domain model. The remainder of this chapter will give a synopsis of frequency-domain analysis and will discuss additional computational enhancements.

3.4 A Synopsis of Frequency Domain Analysis

At this point, the frequency-domain solution to steady-state and transient problems may be outlined as shown in Figure 3.1. The outline emphasizes the fact that $[G_k]$, an $n \times n$ complex matrix, must be formed and inverted for each of the K discrete values of s. For a general loading condition where $K=128$ or 256. These

inversions may drive the cost of the analysis prohibitively high. This is the most fundamental computational problem to overcome when using frequency-domain analysis techniques.

In an attempt to bring the cost of the analysis down, the following suggestions to improve computational efficiency will be considered:

- The reduction of K
- The formation of $[H_k]$ directly (i.e. without calculating $[G_k]$ and inverting it to obtain $[H_k]$)
- The movement of as many calculations as possible outside of the frequency loop
- The reduction of the size of the matrices within the frequency loop

The first suggestion may be evaluated by studying the properties of the DFT of a real function. The study reveals that when a real function is transformed using the DFT, the real part of the frequency spectrum has even symmetry about the Nyquist frequency, and the imaginary part of the spectrum has odd symmetry about the Nyquist frequency. Therefore, only the first K' points of the response function need to be calculated, where

$$K' = \frac{K}{2} + 1 \qquad (3.19)$$

The remainder of the response spectrum may be determined from

$$\{X_k\} = \{X_{K-k}\}^* \qquad k = K'+1,\ldots,K-1 \qquad (3.20)$$

where $\{X_{K-k}\}^*$ is the complex conjugate of $\{X_{K-k}\}$. Therefore, the effective K has been reduced to approximately half of its original value.

The second and third suggestions will be evaluated in the following section, and the fourth suggestion will be evaluated in Section 3.6.

3.5 Forming the Dynamic Flexibility Matrix Directly

Forming the dynamic flexibility matrix directly can lead to a more efficient solution by allowing more computations to be placed outside the frequency loop. It also eliminates the inversion of the complex dynamic stiffness matrix. While the procedure described in this section still requires a matrix inversion, the equations forming the matrix are uncoupled yielding a diagonal matrix whose inversion is trivial.

The direct formulation of the dynamic elasticity matrix will begin by writing the eigenproblem for the undamped structures,

$$\left[-w^2\,[m] + [k]\right]\{x(w)\} = \{0\} \qquad (3.21)$$

A nontrivial solution of Eq. (3.21) may be obtained by setting

$$\det\left|-w^2\,[m] + [k]\right| = 0 \qquad (3.22)$$

and finding the roots. The roots obtained are the n eigenvalues of the system of equations in Eq. (3.21), which have n eigenvectors associated with them. The eigenvectors, ϕ, are stored columnwise in a matrix which is denoted as Φ.

$$[\Phi] = [\phi_1, \phi_2, \ldots, \phi_n] \tag{3.23}$$

Equation (3.7) can now be transformed from physical space to modal space by using the transformation

$$\{X_k\} = [\Phi] \{\eta_k\} \tag{3.24}$$

Substituting this into an expanded form of Eq. (3.7) and premultiplying by $[\Phi]^T$, the equations of motion in modal coordinates can be written as

$$\left[[M] s_k^2 + [C] s_k + [K] \right] \{\eta_k\} = [\Phi]^T \{F_k\} \tag{3.25}$$

where $[M]$ and $[K]$ are $n \times n$ diagonal matrices commonly denoted as the generalized mass and stiffness matrices. The $n \times n$ matrix $[C]$ will only be a diagonal matrix for special types of damping, where it can be shown that

$$[c] [m]^{-1} [k] = [k] [m]^{-1} [c] \tag{3.26}$$

(Ref. 13).

If Eq. (3.26) is satisfied, the equations of motion are uncoupled for each modal degree of freedom. At this point, Eq. (3.25) may be written in simplified form as

$$[A_k]\ \{\eta_k\} = [\Phi]^T\ \{F_k\} \tag{3.27}$$

where

$$[A_k] = \underset{i=1,n}{\text{diag}}\ (M_i s_k^2 + C_i s_k + K_i) \tag{3.28}$$

Equation (3.27) may then be solved for $\{\eta_k\}$ using the following equation

$$\{\eta_k\} = [A_k]^{-1}\ [\Phi]^T\ \{F_k\} \tag{3.29}$$

However, since $[A_k]$ is a diagonal matrix, its inverse consists simply of the reciprocal of the diagonal terms.

The equations may then be transformed back to physical space using the transformation in Eq. (3.24)

$$\{X_k\} = [\Phi]\ [D_k]\ [\Phi]^T\ \{F_k\} \tag{3.30}$$

where

$$[D_k] = [A_k]^{-1} = \underset{i=1,n}{\text{diag}}\ \left(\frac{1}{M_i s_k^2 + C_i s_k + K_i}\right) \tag{3.31}$$

Upon comparing Eqs. (3.11) and (3.30), it is realized that $[H_k]$ may be calculated directly by

$$[H_k] = [\Phi]\ [D_k]\ [\Phi]^T \tag{3.32}$$

Since the eigensolution and the formulation of the generalized mass, stiffness, and damping matrices are clearly frequency-independent; those operations may be placed outside of the frequency loop. It

should be noted, however, that the modal formulation of $[H_k]$ did not come without considerable expense. The major disadvantages of the modal formulation are:

- An $n \times n$ eigensolution must be performed.
- The class of problems has been restricted to those whose damping matrix is diagonalized by the eigenvectors.

However, the advantage of the modal formulation is:

- An $n \times n$ inverse is no longer required at each discrete frequency.

These advantages and disadvantages must be weighed against each other for a particular problem. It is clear that if the equations need to be evaluated at only a single discrete frequency, the single inverse of $[G_k]$ would be more efficient than the eigensolution and subsequent matrix multiplications.

3.6 Reducing the Problem

The next suggestion to improve computational efficiency is the reduction of the size of the matrices in the frequency loop. Recall that n is the number of degrees of freedom of the finite element model, and it cannot be reduced without reducing the accuracy of the solution. However, if the system response is desired at only a limited number of points, the number of system equations can be reduced without reducing the accuracy of the solution.

The reduction process is initiated by partitioning the response vector into those degrees of freedom which are desired, R , and those which are not desired, I . The R-set will be denoted as the relevant set, and the I-set will be denoted as the irrelevant set (i.e. irrelevant in the sense that the response is not desired at those degrees of freedom).

The partitioning yields

$$\{X\} = \begin{Bmatrix} X_R \\ X_I \end{Bmatrix} \tag{3.33}$$

Equation (3.15) may now be partitioned and written as

$$\begin{Bmatrix} X_R \\ X_I \end{Bmatrix} = \begin{bmatrix} H_{RR} & H_{RI} \\ H_{IR} & H_{II} \end{bmatrix} \begin{Bmatrix} F_R \\ F_I \end{Bmatrix} \tag{3.34}$$

The response of the relevant degrees of freedom may be obtained by expanding the top equation, and writing it as

$$\{X_R\} = [H_{RR}]\{F_R\} + [H_{RI}]\{F_I\} \tag{3.35}$$

The problem may be simplified further by requiring all forces to be in the R-set. This will cause the $\{F_I\}$ vector to be a null vector, and will allow Eq. (3.35) to be written as

$$\{X_R\} = [H_{RR}]\{F_R\} \tag{3.36}$$

or

$$\{\bar{X}\} = [\bar{H}]\{\bar{F}\} \tag{3.37}$$

or

$$[\bar{G}]\{\bar{X}\} = \{\bar{F}\} \tag{3.38}$$

where the $(\bar{\ })$ notation indicates a matrix which has been reduced to its relevant degrees of freedom. The relevant part of the dynamic elasticity matrix, often called the dynamic elasticity transfer matrix, is a submatrix of the dynamic elasticity matrix, whereas the relevant part of the dynamic stiffness matrix, or dynamic stiffness transfer matrix, is not a submatrix of the dynamic stiffness matrix.

For problems where the number of relevant degrees of freedom, p, is much less than the total number of system degrees of freedom, n, the use of Eq. (3.37) will be considerably more efficient than the use of Eq. (3.11). The efficiency would be even higher, if $[\bar{H}]$ could be found directly (i.e. without forming $[H]$ and removing the relevant portion).

Geering presents the direct formulation of $[\bar{H}]$ which utilizes a projection scheme (Ref 3). However, by expanding Eq. (3.32), it may be shown that each element in the $[H]$, as well as $[\bar{H}]$, matrix may be obtained from

$$H_{ij} = \sum_{r=1}^{n} \phi_{ir}\, \phi_{jr}\, D_r \tag{3.39}$$

where D_r is the r^{th} diagonal element of $[D_k]$ defined in Eq. (3.31) and ϕ_{ir} (or ϕ_{jr}) represents the value at the i^{th} (or j^{th}) row, and r^{th} column of the modal matrix $[\phi]$.

It should be noted at this point that Eq. (3.37) yields an exact solution to Eq. (3.15) at the relevant degrees of freedom. It is

also an exact solution to Eq. (2.1) if the forward transform of the dynamic load and the inverse transform of the dynamic response spectrum are exact. There is, however, an additional reduction which can be made with an acceptable loss of accuracy.

3.7 Further Reduction of the Problem

The final reduction scheme presented in this chapter is the well-known modal approximation (Ref. 14, 15). It is important to note that this is an approximation to the exact solution given by Eq. (3.37). The loss of accuracy, however, is generally considered to be acceptable.

Modal approximation occurs when only N of the n system modes are retained in the modal expansion of the displacement field (where $N < n$). Equation (3.39) may then be written as

$$H_{ij} = \sum_{r=1}^{N} \phi_{ir} \phi_{ir} D_r \tag{3.40}$$

It is important to remember that if a system is reduced to p relevant degrees of freedom, then a minimum of p modes must be retained in the expansion to guarantee the invertibility of $[\bar{H}]$.

If a modal approximation is used, it is suggested that the residual modes also be included in the analysis in order to reduce the loss of accuracy (Ref. 14, 16).

3.8 A Synopsis of Efficient Frequency-Domain Analysis

At this point, the computational improvements may be incorporated into the outline of Figure 3.1. Recall, however, that these

computational improvements are only improvements for a problem which must be evaluated at a large number of discrete frequencies, s_k . The new outline is shown in Figure 3.2

It is clear that the improvements will help reduce the cost of many analyses. The greatest computational concern now is the potentially large eigenvalue problem which must be solved in Step 2. The following chapter on substructure coupling will address this problem.

1. Determine the spectrum of the exponentially-windowed forcing functions at K discrete frequencies (Eq. (3.9))

2. Execute the following frequency loop K times (k index):

   a. Form $[G_k]$ (Eq. (3.8)).

   b. Invert $[G_k]$ to obtain $[H_k]$

   c. Solve for $\{X_k\}$ (Eq. (3.11))

3. Inverse transform $\{X\}$ to obtain $\{\hat{x}\}^*$ and remove the exponential window to obtain $\{x\}^*$ (Eq. (3.13))

Figure 3.1 Outline for frequency-domain analysis

1. Determine the spectrum of the relevant exponentially-windowed forcing functions, $\{\bar{F}\}$, at K discrete frequencies (Eq. (3.9)).

2. Perform an eigenvalue analysis of the structure in order to obtain the modal matrix $[\Phi]$.

3. Form the $[M]$, $[C]$, and $[K]$ matrices.

4. Execute the following frequency loop K' times (k index):

   a. Form $[\bar{H}_k]$ (Eq. (3.38))

   b. Solve for $\{\bar{X}_k\}$ (Eq. (3.37))

5. Inverse transform $\{\bar{X}\}$ to obtain the relevant part of $\{\hat{x}\}^*$ and remove the exponential window to obtain the relevant part of $\{x\}^*$ (Eq. (3.13)).

Figure 3.2 Outline of efficient frequency-domain analysis.

Chapter 4

SUBSTRUCTURE COUPLING IN THE FREQUENCY DOMAIN

4.1 Equations of Motion for the Substructure

Consider a superstructure[1] that has been separated into two or more substructures. For illustration purposes, consider the superstructure and its substructures shown in Figure 4.1.

Note that each substructure retains the same boundary conditions and external forces which it had as a part of the superstructure. In addition, each substructure has coupling forces at its interfaces with other substructures. These coupling forces represent the forces transmitted by adjacent substructures.

The equations of motion may be written independently for each substructure as

$$[G^1]\{X^1\} = \{F^1\} \tag{4.1}$$

and

$$[G^2]\{X^2\} = \{F^2\} \tag{4.2}$$

The set of physical degrees of freedom for each substructure will now be divided into a set of interface or juncture degrees of freedom, J , and a set of external degrees of freedom, E , which will encompass the remaining active degrees of freedom of the substructure. The substructure equations of motion may be written in partitioned form as

---

[1] This paper will denote the entire structural system either as the superstructure, or as substructure 0 .

Substructure 0 (Superstructure)

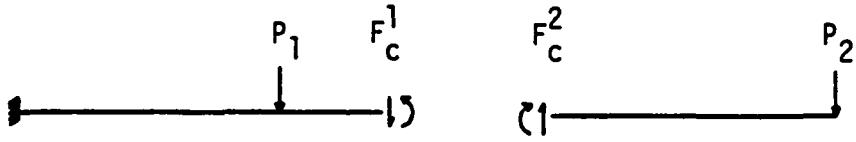

Substructure 1 Substructure 2

Figure 4.1 Typical substructure model.

$$\begin{bmatrix} G^1_{JJ} & G^1_{JE} \\ G^1_{EJ} & G^1_{EE} \end{bmatrix} \begin{Bmatrix} X^1_J \\ X^1_E \end{Bmatrix} = \begin{Bmatrix} F^1_J + F^1_C \\ F^1_E \end{Bmatrix} \tag{4.3}$$

and

$$\begin{bmatrix} G^2_{JJ} & G^2_{JE} \\ G^2_{EJ} & G^2_{EE} \end{bmatrix} \begin{Bmatrix} X^2_J \\ X^2_E \end{Bmatrix} = \begin{Bmatrix} F^2_J + F^2_C \\ F^2_E \end{Bmatrix} \tag{4.4}$$

where the following notation applies to the i^{th} substructure

X^i_J Interface DOFs

X^i_E External DOFs

F^i_C Interface forces due to adjacent substructures

F^i_J External forces at interface DOFs

F^i_E External forces at external DOFs

The frequency-domain equations for each substructure may now be coupled together to form the superstructure equations of motion. This coupling is accomplished by enforcing the displacement and force compatibility at the substructure interfaces.

The displacement compatibility at the interface may be expressed as

$$\{X^1_J\} = \{X^2_J\} = \{X^0_J\} \tag{4.5}$$

Equation (4.5) ensures that the interface displacements of adjacent substructures are identical and are equivalent to the displacement of

the same degrees of freedom on substructure 0 (i.e. the superstructure). Force compatibility at the interface may be written as

$$\{F_C^1\} = -\{F_C^2\} \tag{4.6}$$

At this point, Eqs. (4.3) and (4.4) may be reordered and combined to yield

$$\begin{bmatrix} G_{EE}^1 & G_{EJ}^1 & & \\ G_{JE}^1 & G_{JJ}^1 & & \\ & & G_{JJ}^2 & G_{JE}^2 \\ & & G_{EJ}^2 & G_{EE}^2 \end{bmatrix} \begin{Bmatrix} X_E^1 \\ X_J^1 \\ X_J^2 \\ X_E^2 \end{Bmatrix} = \begin{Bmatrix} F_E^1 \\ F_J^1 + F_C^1 \\ F_J^2 + F_C^2 \\ F_E^2 \end{Bmatrix} \tag{4.7}$$

By adding the second and third equations together, and enforcing the displacement compatibility condition, the system may be reduced to

$$\begin{bmatrix} G_{EE}^1 & G_{EJ}^1 & \\ G_{JE}^1 & (G_{JJ}^1 + G_{JJ}^2) & G_{JE}^2 \\ & G_{EJ}^2 & G_{EE}^2 \end{bmatrix} \begin{Bmatrix} X_E^1 \\ X_J^0 \\ X_E^2 \end{Bmatrix} = \begin{Bmatrix} F_E^1 \\ F_J^1 + F_C^1 + F_J^2 + F_C^2 \\ F_E^2 \end{Bmatrix} \tag{4.8}$$

Now the force compatibility condition may be enforced to yield the equations in their final form (Ref. 3).

$$\begin{bmatrix} G^1_{EE} & G^1_{EJ} & \\ G^1_{JE} & (G^1_{JJ} + G^2_{JJ}) & G^2_{JE} \\ & G^2_{EJ} & G^2_{EE} \end{bmatrix} \begin{Bmatrix} X^1_E \\ X^0_J \\ X^2_E \end{Bmatrix} = \begin{Bmatrix} F^1_E \\ F^1_J + F^2_J \\ F^2_E \end{Bmatrix} \tag{4.9}$$

This process of enforcing compatibility of the forces and displacements at the substructure interfaces is analogous to the direct stiffness approach used in static analysis. The only difference in this dynamic formulation is that the stiffness matrix, displacement vector, and force vector are not constants, but are, instead, functions of frequency.

Extending the analogy of the direct stiffness method, the element stiffness matrix, or the substructure dynamic stiffness matrix, will be defined as

$$[G^i_k] = [m^i]\, s_k^2 + [c^i]\, s_k + [k^i] \tag{4.10}$$

where $[m^i]$, $[c^i]$, and $[k^i]$ are the free-interface mass, damping and stiffness matrices of the i^{th} substructure[2]. Similarly, the element elasticity matrix, or the substructure dynamic elasticity matrix, will be defined as

---

[2] Recall from Chapter 2 that only active degrees of freedom are included in the equations of this paper.

$$[H_k^i] = [\Phi^i]\,[D_k^i]\,[\Phi^i]^T \tag{4.11}$$

where $[\Phi^i]$ is the substructure free-interface modal matrix, and $[D_k^i]$ may be found by substituting the substructure's generalized mass, damping, and stiffness matrices into Eq. (3.31). As demonstrated in Chapter 3, Eq. (4.11) may be expanded and each term of the dynamic elasticity matrix may be expressed as

$$H_{ij}^i = \sum_{r=1}^{n} \phi_{ir}^i \phi_{jr}^i D_r^i \tag{4.12}$$

The number of equations represented by Eq. (4.9) may be calculated by adding together the degrees of freedom of each substructure, m^i, and subtracting the total number of interface degrees of freedom, p_I^o, or

$$n = \sum_{i=1}^{M} m^i - p_I^o \tag{4.13}$$

where M is the total number of substructures.

At this point, it should be noted that Eq. (4.9) is simply a partitioned representation of Eq. (3.14). Therefore, the same solution procedures and modifications described in Chapter 3 are applicable here as well.

4.2 A Synopsis of Substructure Coupling

As in Chapter 3, the above procedure has been outlined in order to determine where the method could be improved upon. An evaluation of

the outline shown in Figure 4.2 again reveals that a reduction in the amount of computation within the frequency loop will yield a more efficient solution to the problem.

The same computational improvements made at the system level apply equally well here, at the substructure level. However, the interface degrees of freedom must now be included in the relevant set in order to provide the coupling to adjacent substructures. Therefore, the relevant set will now consist of interface degrees of freedom as well as forced degrees of freedom and other degrees of freedom where the response is desired.

The substructure coupling outline with the improvements from Chapter 3 is shown in Figure 4.3. An examination of the outline shows that the use of substructures has required additional matrices to be inverted in step 3.a.2. Since the number of calculations required to perform a matrix inversion is on the order of b^3 (where b is the order of the matrix), it is essential that the size of those matrices be reduced.

Recall that $[H^i]$ is a $p^i \times p^i$ matrix, where p^i is the number of relevant degrees of freedom of the i^{th} substructure. It has already been stated that interface degrees of freedom must be included in the relevant set. Therefore, in order to minimize the number of degrees of freedom in the R-set, one must transform all loads to the interface and request the response at only the interface degrees of freedom.

However, requesting the response at the interface degrees of freedom only, is not an acceptable solution, unless the response can be

1. Determine the spectrum of the exponentially-windowed forcing functions at K discrete frequencies (Eq. (3.9)).

2. Execute the following frequency loop K times (k index):

   a. Execute the following substructure loop M times (i index):

      1) Form $[G_k^i]$ Eq. (4.10)

      2) Using direct stiffness methods, sum the $[G_k^i]$ matrices to form $[G_k^o]$, the superstructure dynamic stiffness matrix.

   b. Invert $[G_k^o]$ to obtain $[H_k^o]$

   c. Solve for $\{X_k\}$ (Eq. (3.11))

3. Inverse transform $\{X\}$ to obtain $\{\hat{x}\}^*$ and remove the exponential window to obtain $\{x\}^*$ (Eq. (3.13)).

Figure 4.2 Outline of substructure coupling in the frequency domain.

1. Determine the spectrum of the relevant exponentially-windowed forcing functions at K discrete frequencies (Eq. (3.9)).

2. Execute the following substructure loop M times (i index):
   a. Perform a free-interface eigenvalue analysis of each substructure in order to obtain $[\Phi^i]$.
   b. Form the $[M^i]$, $[C^i]$, and $[K^i]$ matrices.

3. Execute the following frequency loop K' times (k index):
   a. Execute the following substructure loop M times (i index):
      1) Form $[H_k^i]$ (Eq. (4.12))
      2) Invert $[H_k^i]$ to obtain $[G_k^i]$
      3) Using direct methods, sum the $[G_k^i]$ matrices to form $[G_k^o]$, the superstructure dynamic stiffness matrix.
   b. Invert $[G_k^o]$ to obtain $[H_k^o]$
   c. Solve for $\{X_k\}$ (Eq. (3.11))

4. Inverse transform $\{X\}$ to obtain $\{\hat{x}\}^*$ and remove the exponential window to obtain $\{x\}^*$ (Eq. (3.13))

Figure 4.3 Outline of efficient substructure coupling.

recovered subsequently at the irrelevant degrees of freedom. This topic is discussed in the following section. Reducing the loads to interface degrees of freedom is then discussed in section 4.4.

4.3 Recovery of the Response at Irrelevant Degrees of Freedom

Recovery of the irrelevant degrees of freedom may be accomplished by first writing the substructure equations of motion partitioned into their relevant and irrelevant sets

$$\begin{bmatrix} G_{RR} & G_{RI} \\ G_{IR} & G_{II} \end{bmatrix} \begin{Bmatrix} X_R \\ X_I \end{Bmatrix} = \begin{Bmatrix} F_R \\ F_I \end{Bmatrix} \tag{4.14}$$

The bottom equation may then be expanded and solved for the response at the irrelevant degrees of freedom.

$$[G_{IR}] \{X_R\} + [G_{II}] \{X_I\} = \{F_I\} \tag{4.15}$$

$$\{X_I\} = [G_{II}]^{-1} (\{F_I\} - [G_{IR}] \{X_R\}) \tag{4.16}$$

For the special case where all loaded degrees of freedom have been placed in the R-set, $\{F_I\}$ is a null vector and the response of the irrelevant degrees of freedom may be determined using the simplified equation

$$\{X_I\} = -\left[[G_{II}]^{-1} [G_{IR}]\right] \{X_R\} \tag{4.17}$$

where the $\{X_R\}$ vector was determined previously by the evaluation of the superstructure response.

For many problems, this method of calculating response is more efficient than including the desired response points in the system relevant set. As an example, consider two 50 degrees-of-freedom substructures attached at 10 interface degrees of freedom. If the response is desired at each of the 90 system degrees of freedom, and all degrees of freedom were retained in the relevant set, the inversion required in step 3.b of Figure 4.3 would require on the order of 90^3 or 729,000 operations. However, if only the interface degrees of freedom were retained as relevant degrees of freedom, the inversion in step 3.b would be on the order of 10^3 or 1,000 operations. Of course, the subsequent postprocessing required in order to obtain the response at the remaining 80 degrees of freedom would require the inversion of two 40 degree of freedom matrices increasing the cost by another 128,000 operations. However, the total processing cost of the latter method is still considerably less than including all degrees of freedom in the relevant set. However, if the cost of determining the response were to be examined for the same substructures attached at 40 degrees of freedom, one would find that is was more efficient to retain all degrees of freedom in the relevant set.

Although the efficiency of the two methods is problem dependent, the more efficient one may be determined a priori by examining the cost of the inversions required by each of the two methods.

4.4 Transfer of Substructure Loads to the Interface Degrees of Freedom

This final reduction scheme in Chapter 4 will allow all of the substructure's external loads to be transformed into equivalent inter-

face loads. This reduction is very valuable for the class of problems with a large number of external forces (e.g. acoustics, distributed loads, etc.).

This procedure will require another matrix inversion, therefore the system should be reduced so that only interface and loaded degrees of freedom are in the relevant set prior to beginning this reduction. The interface degrees of freedom will again form the J-set, and the remaining degrees of freedom will form the E-set. The substructure equation of motion may then be partitioned and written as

$$\begin{bmatrix} G_{JJ} & G_{JE} \\ G_{EJ} & G_{EE} \end{bmatrix} \begin{Bmatrix} X_J \\ X_E \end{Bmatrix} = \begin{Bmatrix} F_J + F_C \\ F_E \end{Bmatrix} \tag{4.18}$$

Since the interface degrees of freedom will make up the R-set, and the external degrees of freedom will make up the I-set, Eq. (4.18) may be written as

$$\begin{bmatrix} G_{RR} & G_{RI} \\ G_{IR} & G_{II} \end{bmatrix} \begin{Bmatrix} X_R \\ X_I \end{Bmatrix} = \begin{Bmatrix} F_R \\ F_I \end{Bmatrix} \tag{4.19}$$

The bottom equation may be expanded and solved for $\{X_I\}$.

$$\{X_I\} = [G_{II}]^{-1} \left(\{F_I\} - [G_{IR}] \{X_R\}\right) \tag{4.20}$$

At this point, the top equation is expanded using the substitution for $\{X_I\}$ derived above.

$$[G_{RR}]\{X_R\} + [G_{RI}][G_{II}]^{-1}(\{F_I\} - [G_{IR}]\{X_R\}) = \{F_R\} \quad (4.21)$$

Simplifying the notation,

$$[\bar{G}]\{\bar{X}\} = \{\bar{F}\} \quad (4.22)$$

where

$$\{\bar{X}\} = \{X_R\} \quad (4.23)$$

and

$$[\bar{G}] = [G_{RR}] - [G_{RI}][G_{II}]^{-1}[G_{IR}] \quad (4.24)$$

and

$$\{\bar{F}\} = \{F_R\} - [G_{RI}][G_{II}]^{-1}\{F_I\} \quad (4.25)$$

When this reduction scheme is applied to static (i.e. constant) matrices, it is called 'static condensation.' Since the reduction shown above uses dynamic (i.e. not constant) matrices, it is appropriate to call it a 'dynamic condensation.'

It is interesting to note the similarity between Eq. (4.22) and Eq. (3.38). The fact is, they are not only similar, but they are identical. Therefore, the direct formulation of $[\bar{H}]$ may also be viewed as a dynamic condensation of $[G]$ to obtain $[\bar{G}]$, and an inversion to obtain $[\bar{H}]$. This fact will prove useful when determining the natural frequencies of a system which has been reduced to its relevant degrees of freedom.

Chapter 5

DETERMINING THE NATURAL FREQUENCIES OF UNDAMPED STRUCTURES

5.1 The Undamped Free Vibration Problem

The natural frequencies of an undamped structure may be found by examining the free-vibration equations of motion for that structure,

$$[m]\{\ddot{x}\} + [k]\{x\} = \{0\} \tag{5.1}$$

This equation may be transformed to the frequency domain using the methods described in Chapter 2. The free-vibration problem may then be described by the continuous frequency-domain equation

$$[G(s)]\{X(s)\} = \{0\} \tag{5.2}$$

where

$$[G(s)] = [m]s^2 + [k] \tag{5.3}$$

It has been shown that a nontrivial solution to Eq. (5.2) must satisfy the relationship

$$\det |[G(s)]| = 0 \tag{5.4}$$

where $|\cdot|$ is the determinant operator.

An expansion of Eq. (5.4) will yield an n^{th}-order polynomial equation in the complex frequency variable, s^2. It has been shown (Ref. 17) that if [k] and [m] are real, symmetric matrices, where [m] is positive definite and [k] is either positive definite or

positive semi-definite, then the roots of Eq. (5.4) will be purely imaginary. Thus the substitution

$$s = j\omega \tag{5.5}$$

may be used in Eqs. (5.2) and (5.3). However, since s (and therefore $j\omega$) appears in Eq. (5.3) as a squared term only, the equations become purely real and may be written in terms of the real variable ω. Thus

$$[G(\omega)]\ \{X(\omega)\} = \{0\} \tag{5.6}$$

where

$$[G(\omega)] = -\omega^2\ [m] + [k] \tag{5.7}$$

Finally, Eq. (5.4) may be written as

$$\det\ |[G(\omega)]| = 0 \tag{5.8}$$

Either Eq. (5.6) or Eq. (5.8) may be used as the basis for obtaining the natural frequencies of the system as will be shown in the following discussion.

The first approach is to expand Eq. (5.6) and write it in the form of the generalized eigenvalue problem,

$$[k]\ [\Phi] = [m]\ [\Phi]\ [\omega^2] \tag{5.9}$$

The square roots of the n real eigenvalues of this equation are the natural frequencies of the system. There are many algorithms which may be used to solve this generalized eigenvalue problem (Ref. 17, 18). Although a discussion of these algorithms is beyond the scope

of this thesis, the problems associated with obtaining the [m] and [k] matrices will be discussed.

The second approach will address the solution of Eq. (5.8). The algorithms discussed in this paper do not employ the [m] and [k] matrices directly. Instead, the algorithms evaluate the determinant of $[G(\omega)]$ at discrete numerical values of ω. The n positive real values of ω which satisfy Eq. (5.8) are the natural frequencies of the system.

The next section will discuss how the [m] and [k] matrices may be recovered for unreduced frequency-domain problems, and Section 5.3 will explain why the recovery is not practical for a reduced problem. The remaining sections will then discuss the second approach mentioned above.

5.2 Recovering the System Mass and Stiffness Matrices

When using the substructure coupling technique outlined in Section 4.1, the [m] and [k] matrices were not calculated for the superstructure. Only [G] and [H] were known at the system level. It is reasonably simple, however, to recover the system [m] and [k] matrices for this class of frequency-domain problems where the system has not been reduced.

The first step taken to recover the [m] and [k] matrices is to write the equations which define [G] for the undamped system at two distinct frequencies ω_1 and ω_2,

$$[G(\omega_1)] = -\omega_1^2 [m] + [k] \tag{5.10}$$

$$[G(\omega_2)] = -\omega_2^2 [m] + [k] \tag{5.11}$$

Since the mass and stiffness matrices are invariant, they are identical in each of the equations above. Therefore, Eq. (5.11) may be solved for $[k]$,

$$[k] = [G(\omega_2)] + \omega_2^2 [m] \tag{5.12}$$

which may then be substituted into Eq. (5.10) to yield

$$[G(\omega_1)] = -\omega_1^2 [m] + [G(\omega_2)] + \omega_2^2 [m] \tag{5.13}$$

Finally, Eq. (5.13) may be solved for $[m]$ and written as

$$[m] = \frac{[G(\omega_1)] - [G(\omega_2)]}{(\omega_2^2 - \omega_1^2)} \tag{5.14}$$

The $[m]$ and $[k]$ matrices obtained from Eqs. (5.14) and (5.12) may then be used in any suitable eigensolution to obtain the system natural frequencies. It must be noted that although Eqs. (5.12) and (5.14) are algorithmically correct, their stability is not guaranteed for any arbitrary pair of ω which might be chosen.

5.3 Effects of Reduction on the Natural Frequencies

Up to this point, methods of obtaining the natural frequencies have only been considered for systems where all degrees of freedom have been in the relevant set. However, to utilize frequency-domain substructuring techniques effectively, only a minimum number of degrees of freedom are retained in the relevant set.

In Chapter 3, it was determined that the system could be reduced by keeping only the rows and columns of the dynamic elasticity matrix which correspond to the relevant degrees of freedom. It was also shown in Chapter 3 that this reduction scheme is equivalent to a dynamic condensation of the dynamic stiffness matrix.

Since each of the reduction techniques is exact (i.e. no approximations are made), it is reasonable to assume that all of the dynamic characteristics are retained in the dynamic stiffness transfer matrix.

Consider the expansion of $[G]$, given by Eq. (4.24), in terms of the relevant and irrelevant partitions of the $[m]$ and $[k]$ matrices,

$$[G(\omega_k)] = (-\omega_k^2 [m_{RR}] + [k_{RR}]) - (-\omega_k^2 [m_{RI}] + [k_{RI}]) \cdot (-\omega_k^2 [m_{II}] + [k_{II}])^{-1} (-\omega_k^2 [m_{IR}] + [k_{IR}]) \tag{5.15}$$

Although each of the partitions which make up the system $[m]$ and $[k]$ matrices are included in the equations, it is not immediately clear how they could be recovered for use in Eq. (5.9). Furthermore, even if the system $[m]$ and $[k]$ matrices were recovered, an $n \times n$ eigensolution would then be required to obtain the system natural frequencies and the computational advantages of substructuring would be lost.

Therefore, the remainder of the chapter will discuss an alternate solution procedure for determining system natural frequencies which can be extended to handle reduced systems.

5.4 Determining the System Natural Frequencies

Consider Eq. (5.8) upon which this procedure for determining natural frequencies will be based. The expansion of this equation yields an n^{th}-order polynomial in ω^2 . The n positive roots of this polynomial (which is often called the characteristic equation) correspond to the n natural frequencies of the system. A plot of a typical characteristic equation is shown in Figure 5.1.

One of the most popular methods for determining the natural frequencies of a system described by its characteristic equation is the determinant search method (Ref. 18). A pure determinant search method searches for zero crossings of the characteristic polynomial by noting where the determinant of $[G]$ changes sign. Once a root is bracketed (i.e. the determinant is positive on one side of the root and negative on the other side), it is relatively easy to determine its value using a bisection scheme.

There are, however, problems which arise when using a pure determinant search method. They are:

- It is impossible to locate repeated natural frequencies.
- It is difficult to locate closely-spaced natural frequencies.
- It is not possible to determine how many natural frequencies lie within a given frequency range.

From a computational point of view, the method is not very efficient either. The outline for the procedure, shown in Figure 5.2, reveals that the incremental search procedure requires a large number

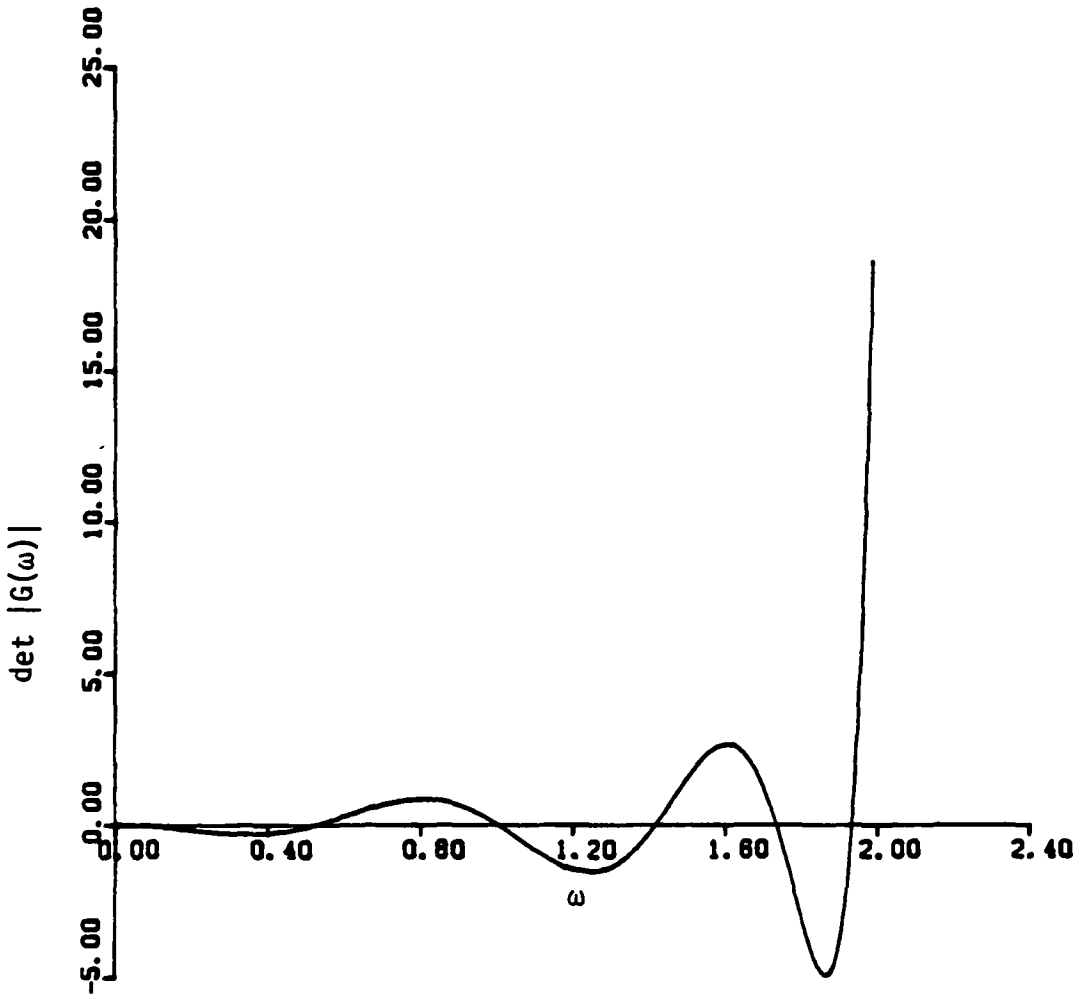

Figure 5.1 Plot of a typical characteristic equation.

1. Initialize DELTA , TOL , ω_{max} , ω_{min}

   DELTA = frequency step
   TOL = tolerance to which natural frequencies are to be determined
   ω_{max} = maximum search frequency
   ω_{min} = minimum search frequency

2. $\omega_{\ell} = \omega_{min}$

3. Form $[G(\omega_{\ell})]$

4. Evaluate $D_{\ell} = \det |G(\omega_{\ell})|$

5. Repeat the following loop to locate roots:

   a. $\omega_u = \omega_{\ell} + DELTA$
   b. Form $[G(\omega_u)]$
   c. Evaluate $D_u = \det |G(\omega_u)|$
   d. If sign (D_{ℓ}) = sign (D_u)
      - Then execute the bisection block
      A. Repeat the following bisection loop:
         1) $\omega = \frac{1}{2}(\omega_{\ell} + \omega_u)$
         2) Form $[G(\omega)]$
         3) Evaluate $D = \det |G(\omega)|$
         4) If sign (D) = sign (D_{ℓ})
            -then $\omega_{\ell} = \omega$; $D_{\ell} = D$
            -else $\omega_u = \omega$; $D_u = D$
         5) DEL = $|\omega_{old} - \omega|$
         6) $\omega_{old} = \omega$
      B. Until DEL < TOL
      C. Report natural frequency found at ω

6. Until $\omega_{\ell} = \omega_{max}$

Figure 5.2 Outline of the pure determinant search method.

of determinants to be evaluated for problems where the search bandwidth is large, but the frequency increment is small in order to be able to bracket closely-spaced natural frequencies. Therefore, the key to reducing the number of determinant evaluations is to come up with a better technique for bracketing the roots.

The following section discusses an enhancement to the determinant search method which solves both the bracketing problem, and the problem the pure method has with locating all of the roots of the characteristic equation.

5.5 Utilizing Sturm Sequence Checks

One of the most popular means of enhancing the determinant search method is by incorporating Sturm sequence checks into the determinant search algorithm. The Sturm sequence check allows each of the problems noted in the previous section to be overcome by determining the number of natural frequencies below a specified frequency. This number, denoted as the Sturm sequence count, S, may then be used in conjunction with a bisection scheme to bracket each zero of the characteristic equation.

A detailed discussion of the Sturm sequence check is beyond the scope of this thesis, and thus the interested reader is referred to the work of Bathe and Wilson (Ref. 18). At this point, it will suffice to know that the Sturm sequence count is equal to the number of negative elements on the diagonal of $[D]$, where $[D]$ is obtained from the $[L][D][L]^T$ decomposition of $[G]$. (Note that the explicit frequency dependency notation has been dropped to simplify the notation.) Thus,

$$S = \sum_{i=1}^{n} c_i \tag{5.16}$$

where

$$c_i = \begin{cases} 1 & \text{if } d_{ii} < 0 \\ 0 & \text{if } d_{ii} \geq 0 \end{cases}$$

where d_{ii} represents the i^{th} term on the diagonal of $[D]$.

The determinant search method utilizing Stürm sequence checks outlined in Figure 5.3 will now be able to located all roots of the characteristic equation, and it will do so with a much higher efficiency than before.

5.6 Determining the Natural Frequencies of Reduced Systems

Up to this point, the determinant search method has only been discussed for unreduced frequency-domain models. However, in order to take full advantage of the computational efficiency of using reduced models, the following extension of the determinant search method is presented.

First, consider the free vibration equations of motion for the undamped system reduced to its relevant degrees of freedom

$$[\bar{G}]\{\bar{X}\} = \{0\} \tag{5.17}$$

In general, a nontrivial solution to this problem must satisfy

$$\det|\bar{G}| = 0 \tag{5.18}$$

1. Initialize TOL , ω_{max} , ω_{min}

2. $\omega_{\ell} = \omega_{min}$; $\omega_{u} = \omega_{max}$

3. Execute the following search loop n times (r index)

   a. Repeat the following bisection loop

      A. $\omega = \frac{1}{2} (\omega_{u} + \omega_{\ell})$

      B. Form $[G(\omega)]$

      C. Decompose $[G(\omega)]$ and determine S

      D. If S < r

         - then $\omega_{\ell} = \omega$

         - else $\omega_{u} = \omega$

      E. DEL = $|\omega_{old} - \omega|$

      F. $\omega_{old} = \omega$

   b. Until DEL < TOL

   c. Report the r^{th} natural frequency

   d. $\omega_{\ell} = \omega$

Figure 5.3 Outline for determining the natural frequencies utilizing Stürm sequence checks

An expansion of Eq. (5.17) and an examination of Figure 5.4 will reveal that the characteristic equation now has poles as well as zeros and is not a simple n^{th}-order polynomial in ω^2 as before. This may be explained by examining Eq. (4.24), which reveals that the poles occur at frequencies where $[G_{II}]$ is singular, and therefore its inverse approaches infinity causing the determinant of $[G]$ to approach infinity also. These frequencies may be thought of as the natural frequencies of the system which has all of its relevant degrees of freedom constrained.

It is obvious that a pure determinant search method would find this environment difficult to work in, since the characteristic equation may now change sign via infinity, as well as via zero. Furthermore, the standard Sturm sequence check will not locate all of the roots either, due to reasons which are detailed in the following discussion.

Since it is the natural frequencies of structures composed of substructures which is of primary interest in this thesis, consider a superstructure which has been reduced such that only the interface degrees of freedom are in the relevant set. The equation of motion describing this system has been stated previously in Eq. (5.17).

As in the previous section, the $p_I^o \times p_I^o$ dynamic stiffness transfer matrix, $[\bar{G}]$, may be factored using an $[\bar{L}][\bar{D}][\bar{L}]^T$ decomposition. By taking into account that the forcing function is a null vector, the decomposed equation of motion may be simplified and written as

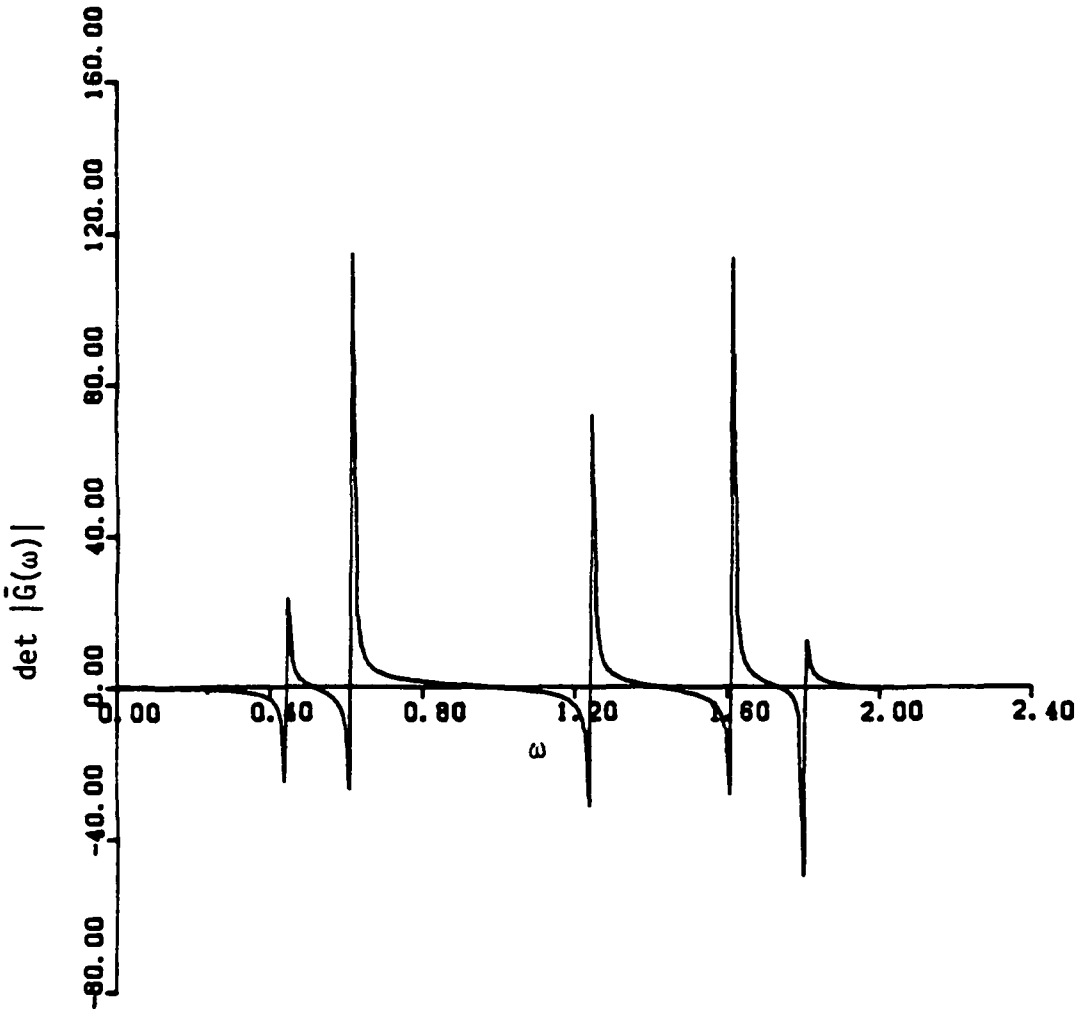

Figure 5.4 Plot of a typical characteristic equation of an undamped system reduced to its relevant degrees of freedom.

$$[\bar{U}]\{\bar{X}\} = \{0\} \tag{5.19}$$

where

$$[\bar{U}] = [\bar{D}][\bar{L}]^T \tag{5.20}$$

and $[\bar{U}]$ is an upper triangular matrix.

The Sturm sequence count of the reduced system may now be obtained by counting the number of negative elements on the diagonal of $[\bar{D}]$. Thus

$$\bar{S} = \sum_{i=1}^{p_I^o} \bar{c}_i \tag{5.21}$$

where

$$\bar{c}_i = \begin{cases} 1 & \text{if } \bar{d}_{ii} < 0 \\ 0 & \text{if } \bar{d}_{ii} \geq 0 \end{cases}$$

and $\bar{d}_{ii}$ represents the i^{th} diagonal element of $[\bar{D}]$. It should be clear at this point, that the maximum attainable Sturm sequence count for this reduced system is p_I^o since there are not more than p_I^o diagonal elements on the diagonal of a $p_I^o \times p_I^o$ matrix.

In order to determine the significance of the Sturm sequence count calculated in Eq. (5.21), write the equations of motion of the unreduced system partitioned into its relevant and irrelevant parts.

$$\begin{bmatrix} G_{II} & G_{IR} \\ G_{RI} & G_{RR} \end{bmatrix} \begin{Bmatrix} X_I \\ X_R \end{Bmatrix} = \begin{Bmatrix} 0 \\ 0 \end{Bmatrix} \tag{5.22}$$

Equation (5.22) may now be decomposed and written in its upper diagonal form,

$$\begin{bmatrix} U_{II} & U_{IR} \\ U_{RI} & U_{RR} \end{bmatrix} \begin{Bmatrix} X_I \\ X_R \end{Bmatrix} = \begin{Bmatrix} 0 \\ 0 \end{Bmatrix} \tag{5.23}$$

Since $[U]$ is an upper triangular matrix, $[U_{RI}] = [0]$ and the bottom equation may be written as

$$[U_{RR}]\{X_R\} = \{0\} \tag{5.24}$$

Recalling that $\{X_R\} = \{\bar{X}\}$, the comparison of Eqs. (5.19) and (5.24) reveals that

$$[\bar{U}] = [U_{RR}] \tag{5.25}$$

Therefore, the Sturm sequence count of the relevant degrees of freedom in Eq. (5.24) is equivalent to the Sturm sequence count of the reduced system in Eq. (5.19) (Ref. 6). Now, only the significance of the Sturm sequence count of the irrelevant degrees of freedom needs to be discussed.

Consider the definition of the Sturm sequence count for the $(n - p_I^o)$ degrees of freedom in the irrelevant set.

- The Sturm sequence count for the $(n - p_I^o)$ degrees of freedom is equivalent to the total number of fixed-interface substructural natural frequencies which are less than the specified frequency.

Thus, the count for the irrelevant degrees of freedom may be written as

$$S_{SB}^{j} = \sum_{r=1}^{m^j - p^j} \tilde{c}_r^j \tag{5.26}$$

where

$$\tilde{c}_r^j = \begin{cases} 1 & \text{if } \omega_r^j < \hat{\omega} \\ 0 & \text{if } \omega_r^j \geq \hat{\omega} \end{cases}$$

and ω_r^j represents the r^{th} fixed-interface natural frequency of the j^{th} substructure, and $\hat{\omega}$ is the frequency at which the count is to be determined.

In summary, the effective Stürm sequence count, S, may be determined by

$$S = \bar{S} + \sum_{j=1}^{M} S_{SB}^{j} \tag{5.27}$$

This effective Stürm sequence count is equivalent to the Stürm sequence count obtained by Eq. (5.16) for the unreduced system, and it may be used in conjunction with a bisection scheme to determine the natural frequencies of the superstructure.

5.7 Conclusions

This method of determining the natural frequencies of a superstructure using frequency-domain substructure models has both advantages and disadvantages over the time-domain methods.

The advantages are:

- There are no large superstructure eigensolutions to perform.

- The method allows for the calculation of only a specified number of natural frequencies (e.g. the first 10 natural frequencies) or the natural frequencies within a given frequency range.

and the primary disadvantage is:

- The fixed-interface natural frequencies must be determined for each of the substructures using an eigensolution or other suitable method.

It must be remembered however, that the number of calculations involved in an eigensolution is greater than n^3 . Therefore, the cost of several small eigensolutions plus the cost of the frequency-domain search described in this section is often less than that required to perform the superstructure eigensolution. As illustrated in Section 4.3, the cost of the analysis is dependent upon the number of interface degrees of freedom and other problem-dependent parameters.

Chapter 6

DETERMINING THE NATURAL FREQUENCIES OF DAMPED STRUCTURES

6.1 The Damped Free Vibration Problem

The natural frequencies of damped structures may be found using a frequency-domain technique similar to the one discussed in Chapter 5. The development of the technique will follow a path similar to that in Chapter 5 and begins by first writing the free-vibration equations of motion for a damped structure in the time domain,

$$[m]\{\ddot{x}\} + [c]\{\dot{x}\} + [k]\{x\} = \{0\} \tag{6.1}$$

and in the frequency domain,

$$[G(s)]\{X(s)\} = \{0\} \tag{6.2}$$

where

$$[G(s)] = [m]s^2 + [c]s + [k] \tag{6.3}$$

As in Chapter 5, a nontrivial solution to this equation must satisfy

$$\det |G(s)| = 0 \tag{6.4}$$

This equation may also be expanded to yield an n^{th}-order polynomial equation in s^2 having $2n$ roots. However, with the inclusion of the damping matrix, the roots may be complex as well as real.

Either Eq. (6.2) or Eq. (6.4) may be used to obtain the damped natural frequencies of the system. However, the solution of Eq. (6.2)

is subject to the same problems of obtaining the system mass and stiffness matrices of reduced systems as seen in Chapter 5. Therefore, this chapter will concentrate on the solution of Eq. (6.4) which is more applicable to frequency-domain models.

6.2 Determining the Damped Natural Frequencies of Reduced Systems

Since it is the determination of natural frequencies of reduced systems which is of primary interest in this thesis, this discussion will begin by considering the reduced frequency-domain equations of motion for a damped system

$$[\bar{G}]\ \{\bar{X}\} = \{0\} \tag{6.5}$$

Although this equation appears identical to Eq. (5.17), the $p_I^o \times p_I^o$ dynamic stiffness transfer matrix is now complex instead of real as it was in Chapter 5. Since the transfer matrix is complex, a general nontrivial solution must now satisfy

$$\det |\bar{G}(s)| = 0 \tag{6.6}$$

where both the real and imaginary parts of the determinant are zero.

This chapter will also employ a determinant search technique to solve Eq. (6.6). However, the search for the roots must now be made in the complex s-plane, whereas in Chapter 5, it was made only along the imaginary axis of the s-plane.

The search for the $2n$ complex roots may be restricted to the positive imaginary half-plane by noting that if a complex root is a solution to Eq. (6.6), then the complex conjugate of the root is also a

solution. Therefore, the search may be restricted to quadrants I and II of Figure 6.1. The search may be restricted further by noting that for conservative systems, the real part of the natural frequency must be less than zero, and therefore, the search may be restricted to quadrant II.

A pure determinant search method for locating the roots of Eq. (6.4) in the complex plane is subject to the same problems with identifying repeated roots and closely-spaced roots as before. It is also possible that the determinant will change signs via infinity as before, as shown in Figure 6.2. Therefore an index-checking scheme similar to the Stürm sequence checks used in Chapter 5 is also desirable when searching for roots in the complex plane.

6.3 Extending Stürm Sequence Checks to the Complex Plane

An examination of the derivation of the Stürm sequence check reveals that one of the most fundamental properties upon which the method is based is the eigenvalue separation property of undamped systems. The property may be stated as (Ref. 18)

$$\omega_1^{<k>} \leq \omega_1^{<k+1>} \leq \omega_2^{<k>} \leq \omega_2^{<k+1>} \cdots \leq \omega_{n-k-1}^{<k>} \leq \omega_{n-k-1}^{<k+1>} \leq \omega_{n-k}^{<k>} \qquad (6.7)$$

$$k = 0, 1, 2 \ldots n-2$$

In essence, the property says that applying an additional constraint to the system will cause the eigenvalues of the constrained system to fall between those of the system without the additional constraint.

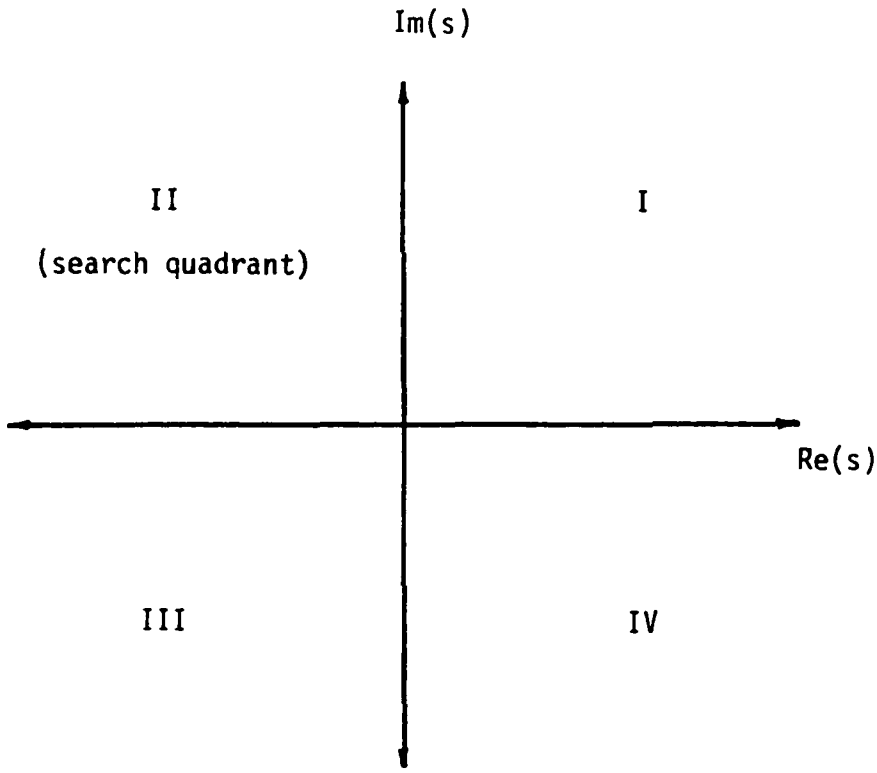

Figure 6.1 Quadrants of the complex plane.

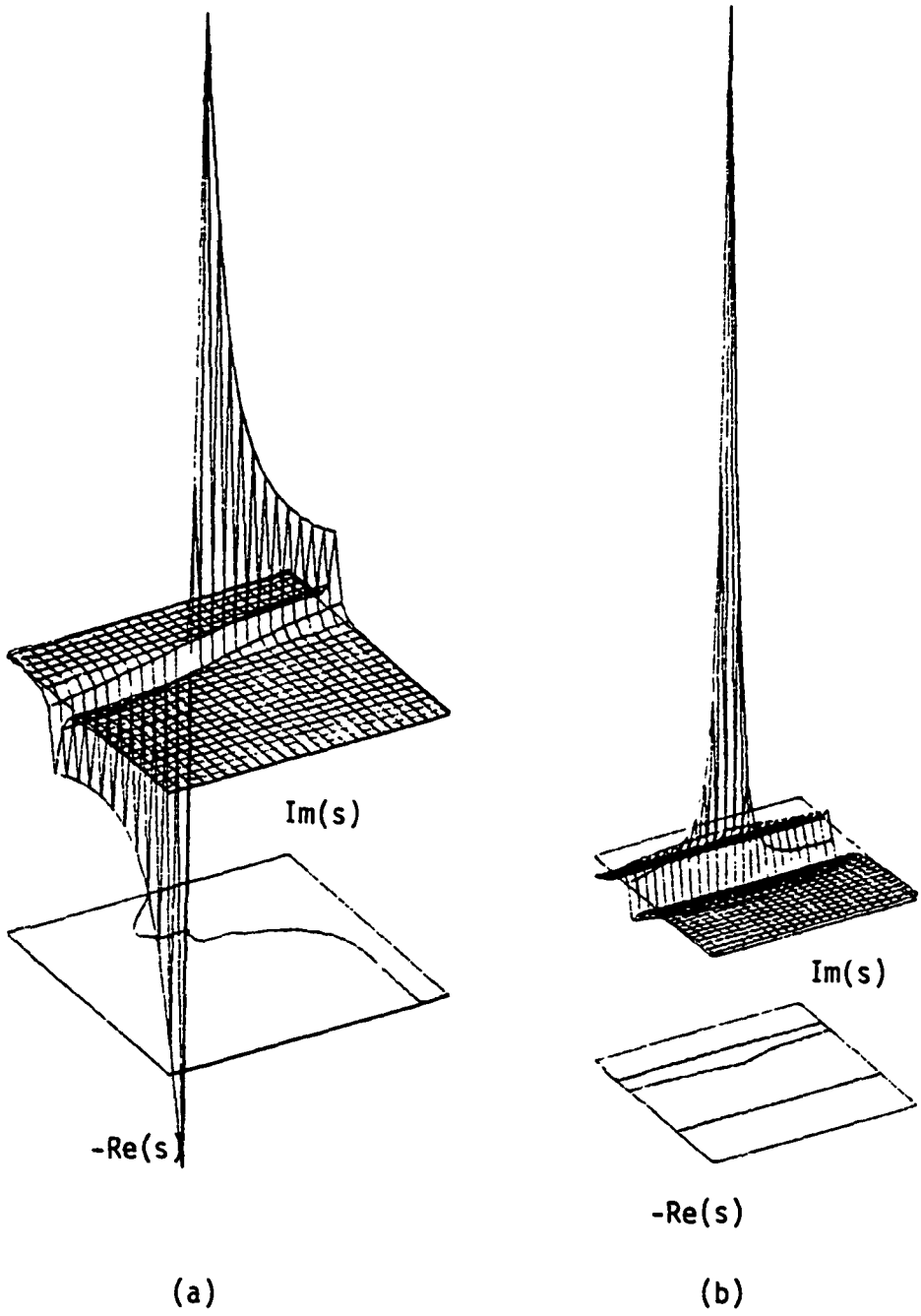

Figure 6.2 Three dimensional plots and contours of the (a) real and (b) imaginary parts of a typical characteristic equation of a damped system reduced to its relevant degrees of freedom.

Although the separation property was derived for an undamped system, it will be assumed that it can be extended to damped systems by the following

$$|\text{Re}\ (s_1^{<k>})| \leq |\text{Re}\ (s_1^{<k+1>})| \leq |\text{Re}\ (s_2^{<k>})| \cdots \qquad (6.8)$$

and

$$|\text{Im}\ (s_1^{<k>})| \leq |\text{Im}\ (s_1^{<k+1>})| \leq |\text{Im}\ (s_2^{<k>})| \cdots \qquad (6.9)$$

where s_r is the r^{th} damped natural frequency (i.e. $s_r = a_r - j\omega_r$) . A mathematical proof of Eqs. (6.8) and (6.9) is beyond the scope of this thesis; therefore, the equations are presented without proof. However, an example will be presented in Chapter 7 which will demonstrate the applicability of the equations to one particular system.

Recall that for the undamped system, the dynamic stiffness matrix [G] is real, and that the Stürm sequence check was used to locate the imaginary parts of the roots (the real parts were known to be zero). Although [G] is complex for the damped system, Eq. (6.9) will permit the Stürm sequence check to be used to determine the imaginary part of the root from the real part of the triangularized [G] matrix. Likewise, Eq. (6.8) will permit the Stürm sequence count of the imaginary part of the triangularized [G] to be used to obtain the real part of the root. The above statements may be expressed as

$$S^I = \sum_{i=1}^{n} c_i \qquad (6.10)$$

where

$$c_i = \begin{cases} 1 & \text{if } \mathrm{Re}\,(d_{ii}) < 0 \\ 0 & \text{if } \mathrm{Re}\,(d_{ii}) \geq 0 \end{cases}$$

and

$$S^R = \sum_{i=1}^{n} b_i \tag{6.11}$$

where

$$b_i = \begin{cases} 1 & \text{if } \mathrm{Im}\,(d_{ii}) < 0 \\ 0 & \text{if } \mathrm{Im}\,(d_{ii}) \geq 0 \end{cases}$$

where d_{ii} is the i^{th} term of the diagonal matrix resulting from the $[L][D][L]^T$ decomposition of $[G]$.

Reduction of the system and substructuring presents the same problems for the damped system as for the undamped. An argument similar to the one used in Section 5.6 may be used to derive the Sturm sequence counts for the damped system with substructures. For the sake of brevity, only the final equations are presented here.

The Sturm sequence count which will be used to determine the imaginary part of the root may be written as

$$S^I = \bar{S}^I + \sum_{j=1}^{M} (S^I_{SB})^j \tag{6.12}$$

where

$$\bar{S}^I = \sum_{i=1}^{p^o_I} \bar{c}_i \tag{6.13}$$

$$\bar{c}_i = \begin{cases} 1 & \text{if } \mathrm{Re}\,(\bar{d}_{ii}) < 0 \\ 0 & \text{if } \mathrm{Re}\,(\bar{d}_{ii}) \geq 0 \end{cases}$$

and

$$(S_{SB})^j = \sum_{r=1}^{m^j - p^j} \tilde{c}_r^j \tag{6.14}$$

$$\tilde{c}_r^j = \begin{cases} 1 & \text{if } \mathrm{Im}\,(s_r) < 0 \\ 0 & \text{if } \mathrm{Im}\,(s_r) \geq 0 \end{cases}$$

Similarly, the Sturm sequence count which will be used to determine the real part of the root may be written

$$S^R = \bar{S}^R + \sum_{j=1}^{M} (S_{SB}^R)^j \tag{6.15}$$

where

$$\bar{S}^R = \sum_{i=1}^{p_I^o} \bar{b}_i \tag{6.16}$$

$$\bar{b}_i = \begin{cases} 1 & \text{if } \mathrm{Im}\,(\bar{d}_{ii}) < 0 \\ 0 & \text{if } \mathrm{Im}\,(\bar{d}_{ii}) \geq 0 \end{cases}$$

and

$$(S_{SB})^j = \sum_{r=1}^{m^j - p^j} \tilde{b}_r^j \tag{6.17}$$

$$\tilde{b}_r^j = \begin{cases} 1 & \text{if } \mathrm{Re}(s_r) < 0 \\ 0 & \text{if } \mathrm{Re}(s_r) \geq 0 \end{cases}$$

The next section describes an algorithm which has been implemented to demonstrate the applicability of Eqs. (6.8) and (6.9) in finding complex natural frequencies. The algorithm utilizes the Stürm sequence counts obtained in Eqs. (6.12) and (6.15).

6.4 Bisection in the Complex Plane

The damped natural frequencies may now be determined using the Stürm sequence indices given by Eqs. (6.12) and (6.15). However, a simple bisection scheme will no longer suffice for determining the roots, since the bisection of a plane is not unique. One relatively simple method of determining the roots is to combine a bilinear search algorithm with a bisection algorithm.

The objective of the search is to find the value of s in the complex plane where both S^R and S^I change from (r-1) to (r) when looking for the r^{th} root. This frequency, s, corresponds to the r^{th} natural frequency of the system. Figure (6.3) has been included to demonstrate how the Stürm sequence counts vary in the search quadrant of the complex plane.

In short, as the bilinear search algorithm is looking for the r^{th} root, it holds the real part of s constant and then uses bisection to obtain an estimate of the imaginary real part of the r^{th} root. It then holds the imaginary part of s constant and uses bisection to obtain an estimate of the real part of the root. This procedure is

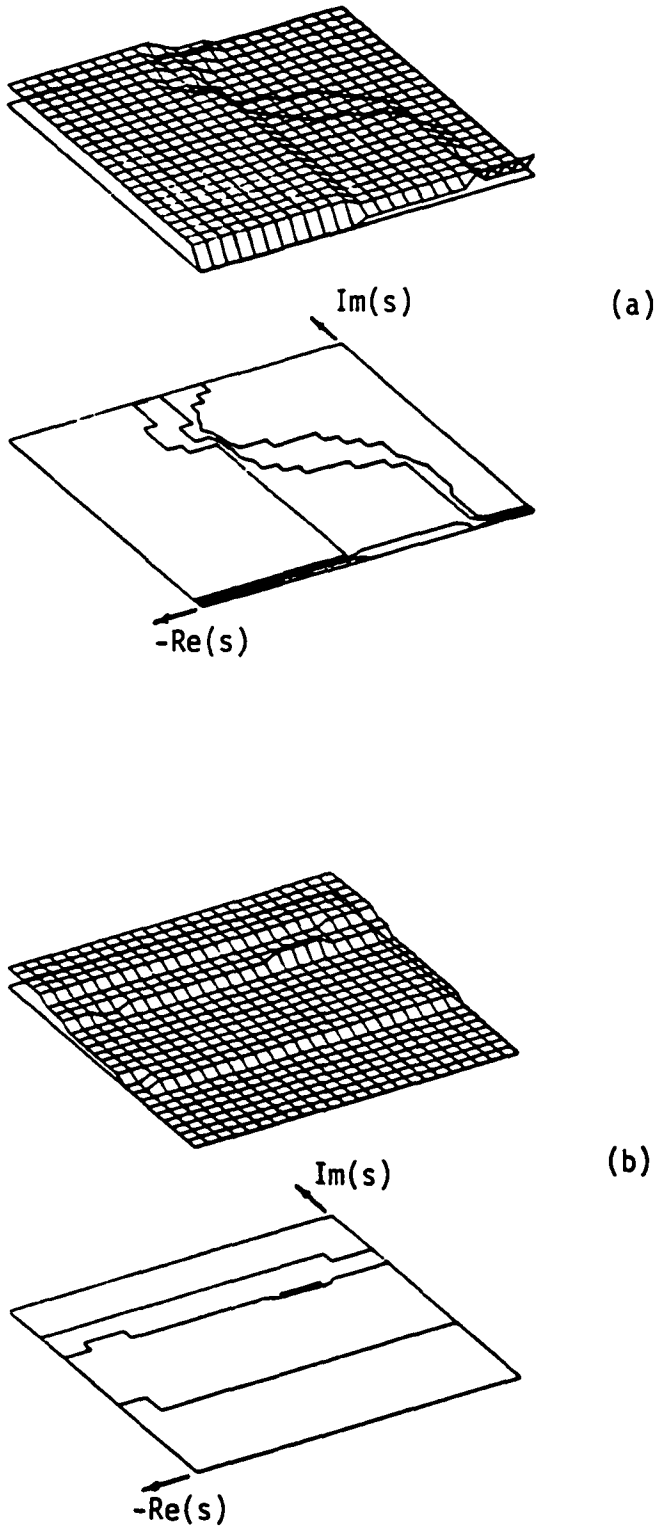

Figure 6.3 Stürm sequence counts, (a) S^R and (b) S^I plotted in the complex plane.

then repeated until both searches satisfy the tolerances specified. The value of s at which both tolerances are satisfied is the r^{th} damped natural frequency of the superstructure.

6.5 Conclusions

From a computational standpoint, the advantages and disadvantages of using frequency-domain techniques instead of time-domain techniques to determine the damped natural frequencies of a system are similar to those listed in Section 5.7 for an undamped system. The only significant difference is that the damped natural frequencies are now required for each fixed interface substructure.

From a practical standpoint, the primary concern with using this frequency-domain method is that Eqs. (6.8) and (6.9) have not been proven explicitly. The numerous examples which have been examined by the author have been successful. However, this is not a proof that the equations are valid for all systems.

Chapter 7

EXAMPLES

7.1 Introduction

This chapter has been included to demonstrate some of the frequency-domain techniques discussed in previous chapters. The examples do not detail the computations involved in the analysis of a problem, but instead they outline the major steps in each of the frequency domain analysis techniques and demonstrate the selection of proper analysis parameters.

The following examples are included:

Example 1 - This example demonstrates how the transient response may be determined using frequency-domain techniques, and the importance of selecting the proper sampling parameters.

Example 2 - This example demonstrates the coupling of substructures in the frequency domain and provides additional details on the selection of sampling parameters.

Example 3 - This example demonstrates how the natural frequencies of undamped superstructures may be obtained using frequency domain substructure models.

Example 4 - This example demonstrates the applicability of Eqs. (6.8) and (6.9) for determining the damped natural frequencies of a superstructure using frequency domain substructure models.

Example 1

The first example will demonstrate the importance of careful selection of the sampling parameters as discussed in Chapter 3. The structure to be used in this example is the simple 1-DOF mass-spring oscillator

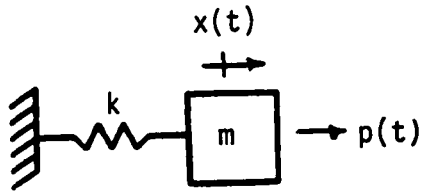

with the following system parameters:

$m = 1.0$ lbs^2/in $\qquad \omega_1 = 31.42$ rads/sec

$k = 987.0$ lb/in $\qquad f_1 = 5.0$ Hz

The transient response of the system to two different dynamic loadings will be determined using the procedures outlined in Chapters 2 and 3.

A. Selecting the Nyquist Frequencies

In order to demonstrate the selection of a proper Nyquist frequency, the structure will be subjected to the cosine pulse loading,

$$p(t) = \begin{cases} 0 & t < 0 \\ 987 \cos(10\pi t) & 0 \leq t \leq 0.05 \\ 0 & t > 0.05 \end{cases}$$

A pulse such as this is not band-limited, and therefore the Nyquist frequency cannot be selected as the highest frequency in the exponentially-windowed pulse. Therefore, the alternate method of determining f_N described in Chapter 3 will be used.

Before proceeding, however, a convergence factor will be selected as the maximum value allowed by Eq. (3.18). Therefore, assuming a 1.0 second response window,

$$T_o = 1.0$$

and

$$a = 4.605$$

Now, in accordance with the procedure outlined in Chapter 3, a value of f_c is selected by examining the system transfer function shown in Figure 7.1. The transfer function is effectively zero for frequencies greater than 50 Hz, thus

$$f_c = 50 \text{ Hz}$$

Figure 7.2 shows the exponentially-windowed force spectra at frequencies less than f_c for several Nyquist frequencies. An examination of the spectra reveals that as the Nyquist frequency increases, the spectra begin to converge to what is assumed to be an exact representation of the exponentially-windowed force spectrum for frequencies less than f_c. For the exponentially-windowed force spectra shown in Figure 7.2, the convergence is good for Nyquist frequencies greater than 512 Hz. Thus,

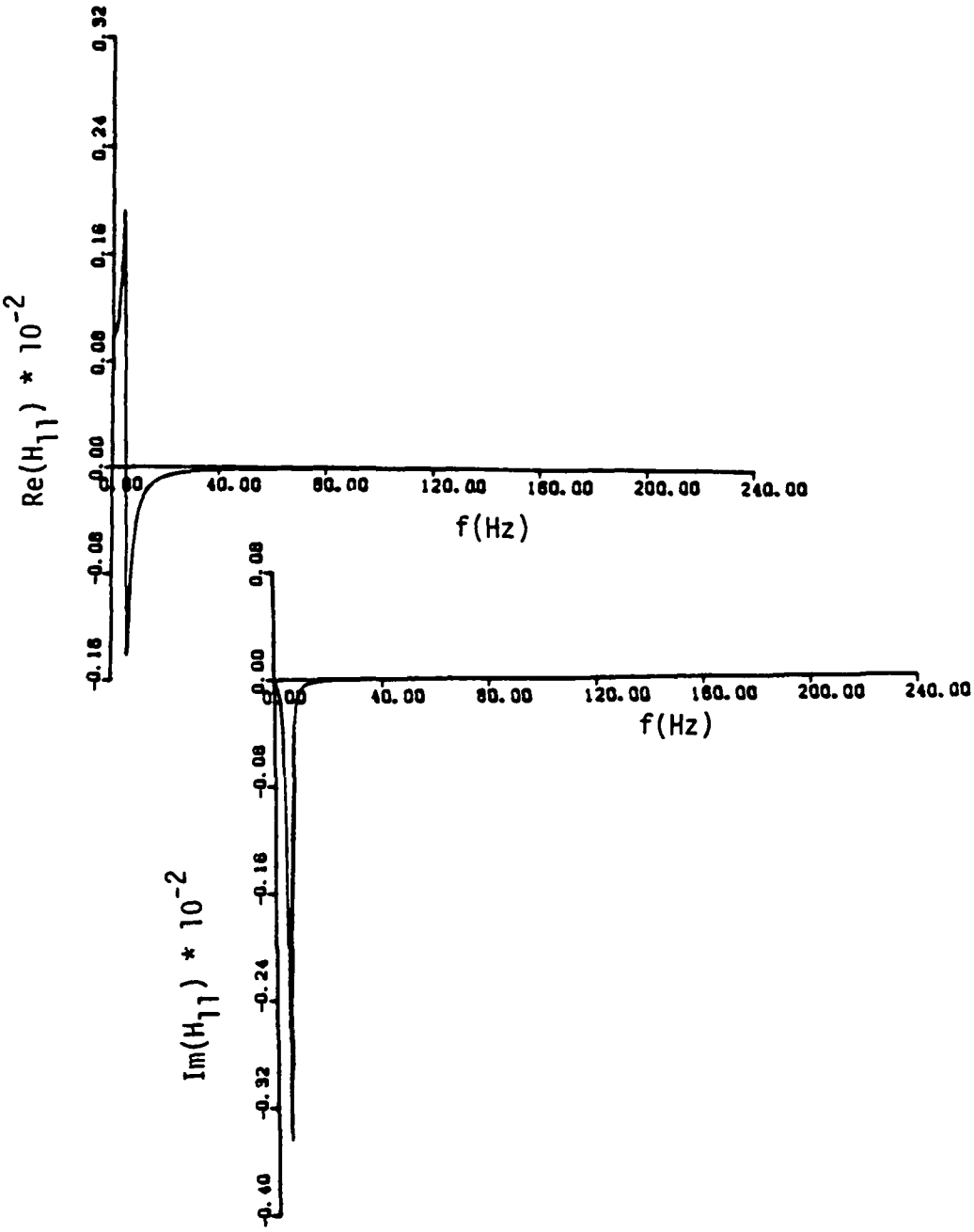

Figure 7.1 System transfer function (a = 7.675)

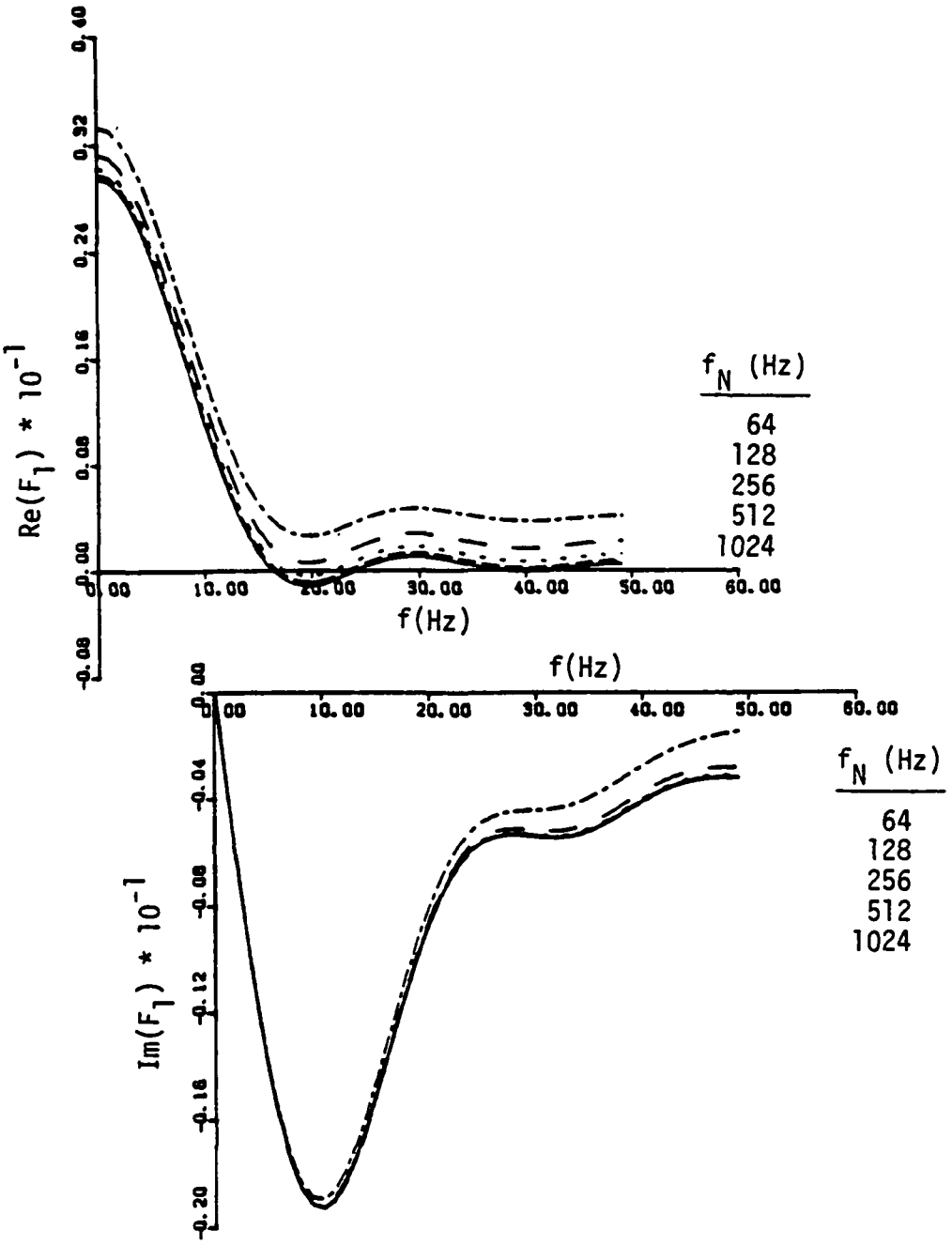

Figure 7.2 Exponentially-windowed force spectra for various Nyquist frequencies.

$$f_N = 512 \text{ Hz}$$

Therefore, having selected T_o and f_N, the remaining sampling parameters may be determined using Eqs. (B.1) through (B.4) in Appendix B,

$K = 1024$ $\qquad$ $f_s = 1024$ Hz

$T = 9.7656 * 10^{-4}$ sec $\qquad$ $f_o = 1.0$ Hz

The system response may now be determined using Eqs. (3.7) through (3.13). The exact solution and the frequency-domain solution have been plotted in Figure 7.3a using the sampling parameters determined above. The two solutions are nearly identical for $f_N = 512$ Hz. However, Figure 7.3b reveals that selecting a Nyquist frequency which is less than that required causes the frequency-domain solution to have a significant error.

B. Selecting a Convergence Factor

In order to demonstrate the selection of a proper convergence factor, the structure used in part A will be subjected to a 1 Hz cosine forcing function. Thus,

$$p(t) = 987.0 * \cos(2\pi t)$$

The system response is desired for t less than 0.6 seconds, thus

$$T = 0.6$$

Selecting the convergence factor to be the maximum allowed by Eq. (3.18) yields

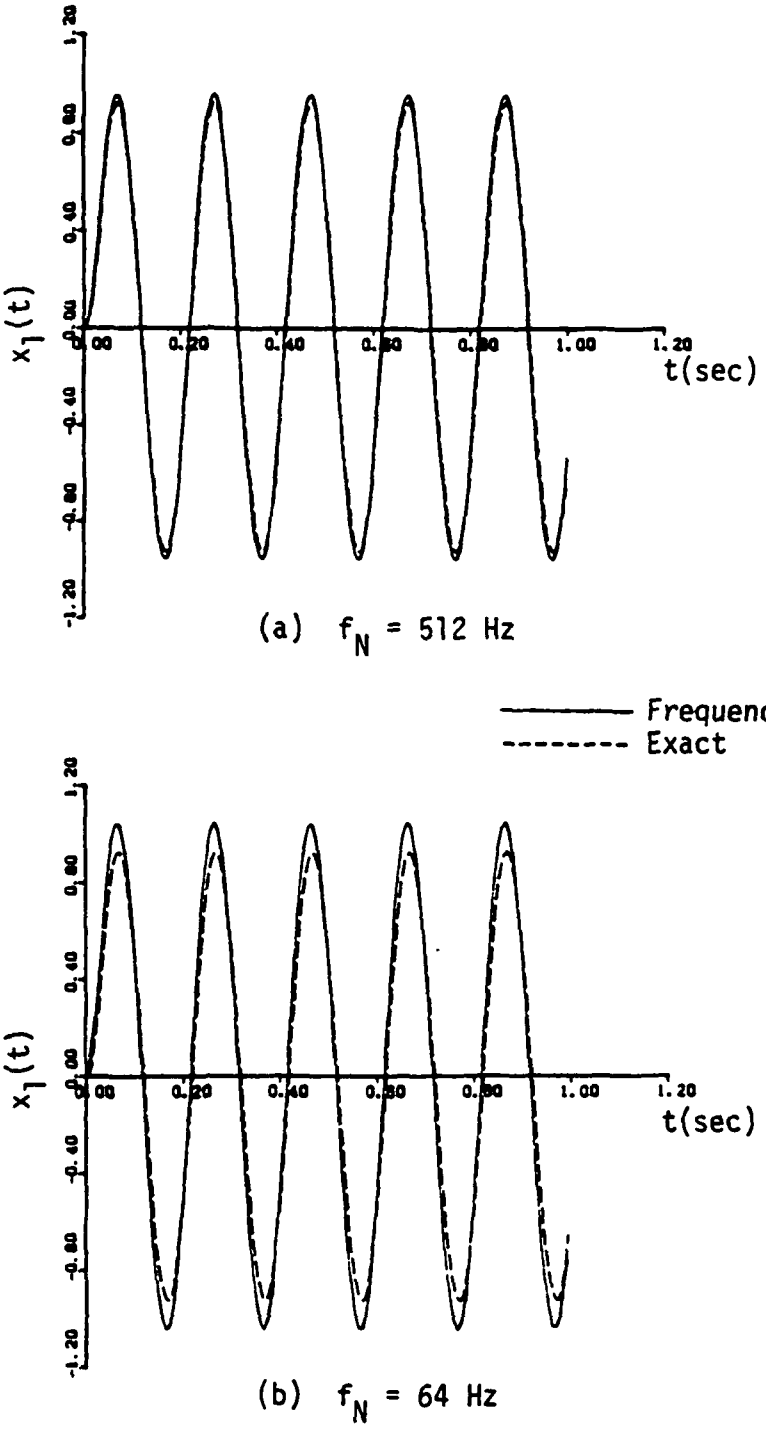

Figure 7.3 System response to cosine pulse excitation.

$$a = 7.675$$

As in the previous example, the spectrum of the exponentially-windowed forcing function shown in Figure 7.4 is examined to determine a suitable Nyquist frequency. Using the same criteria as in the previous example, the Nyquist frequency is chosen to be

$$f = 426.7 \text{ Hz}$$

The remaining sampling parameters may now be determined and the response calculated.

An examination of the exponentially-windowed response, in Figure 7.5a, reveals that the convergence factor selected above has caused the response to decay to 'effectively zero' by the end of the window. Therefore, the frequency-domain response will not be time-aliased. The comparison of the exact and frequency-domain solutions shown in Figure 7.5 supports the statement above, as the solutions are nearly identical.

In order to demonstrate the effectiveness of the convergence factor in preventing time-domain aliasing, the response will be determined using

$$a = 1.0$$

An examination of the exponentially-windowed response in Figure 7.6a reveals that the convergence factor has not caused the windowed response to be 'effectively zero' by the end of the response window. Therefore, as expected, the comparison of the exact and frequency-

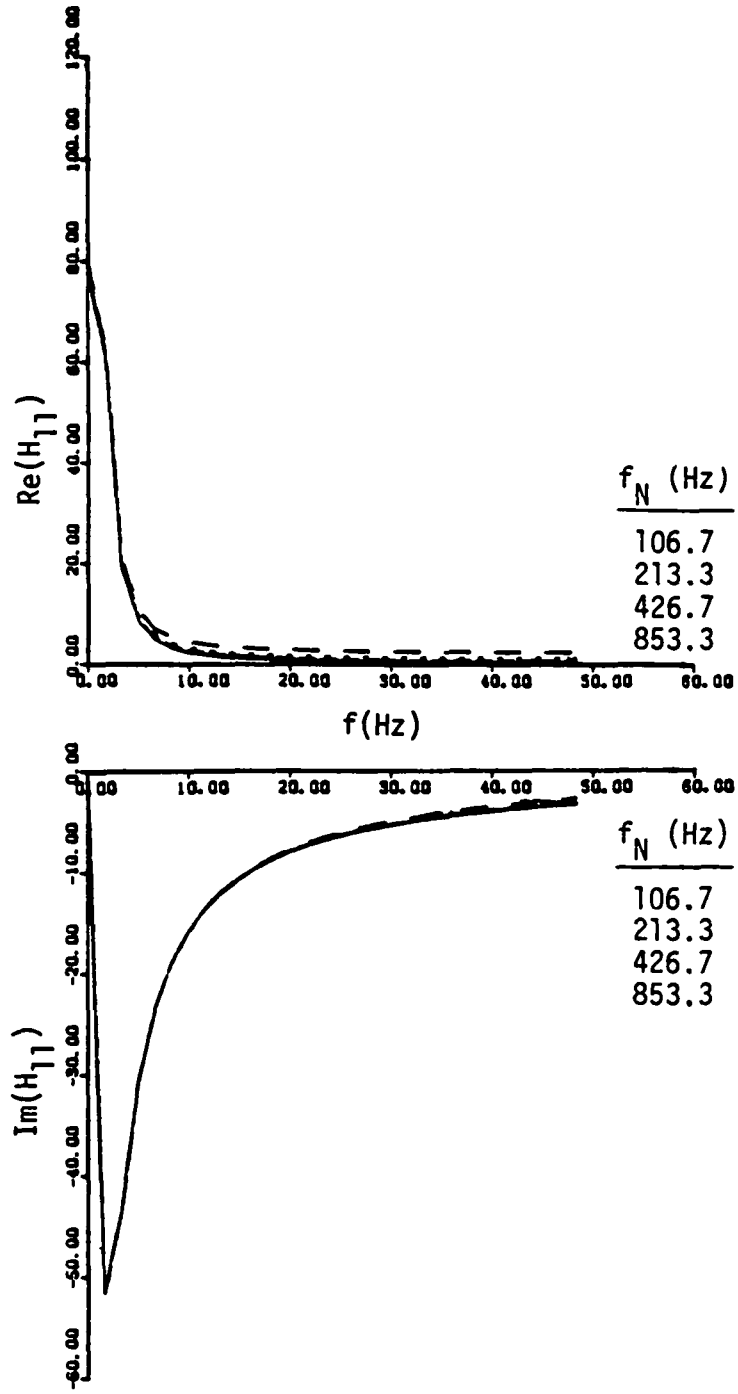

Figure 7.4 Exponentially-windowed force spectra for various Nyquist frequencies.

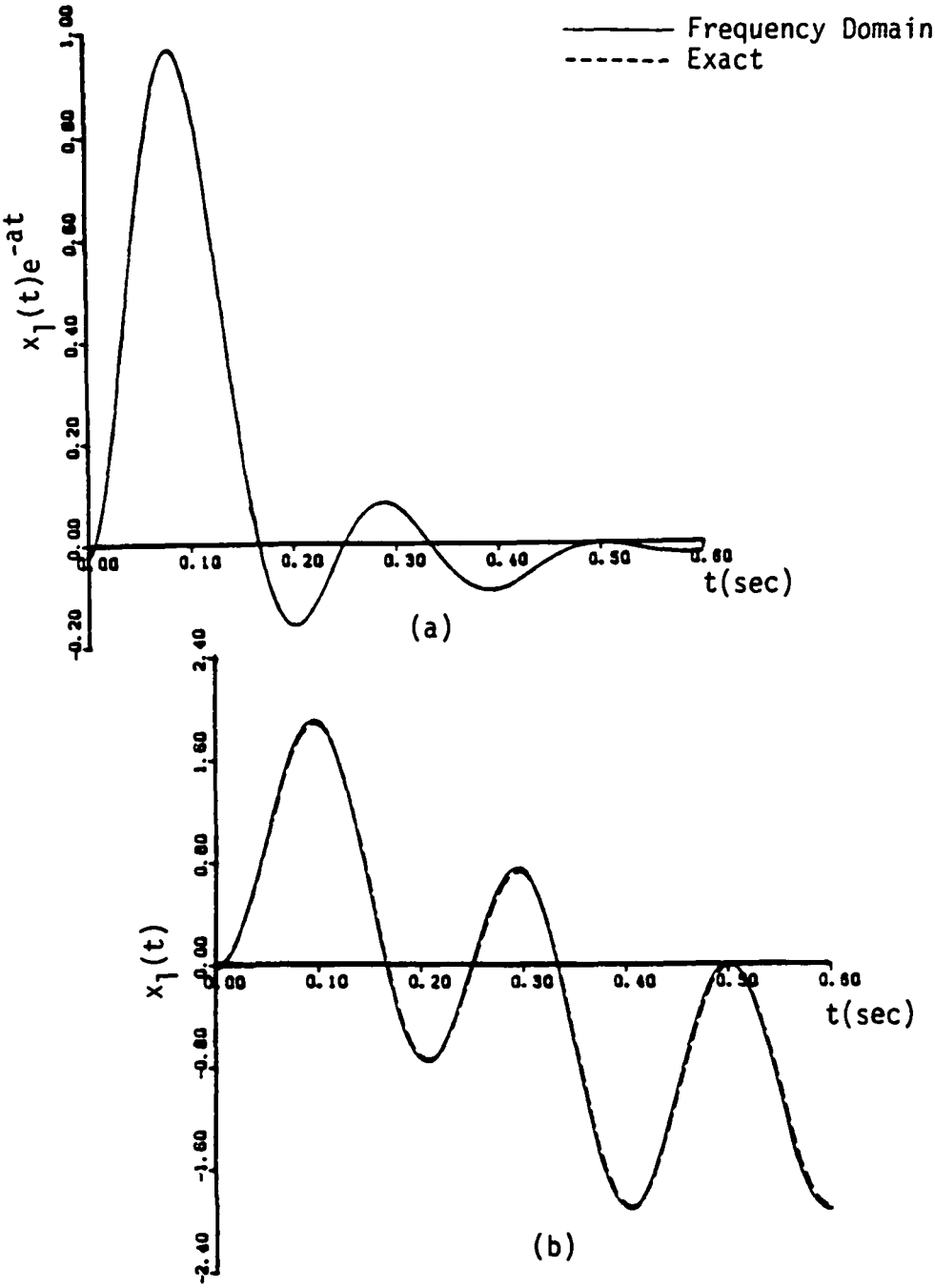

Figure 7.5 (a) Exponentially-windowed response and (b) the response with the window removed (a = 7.675).

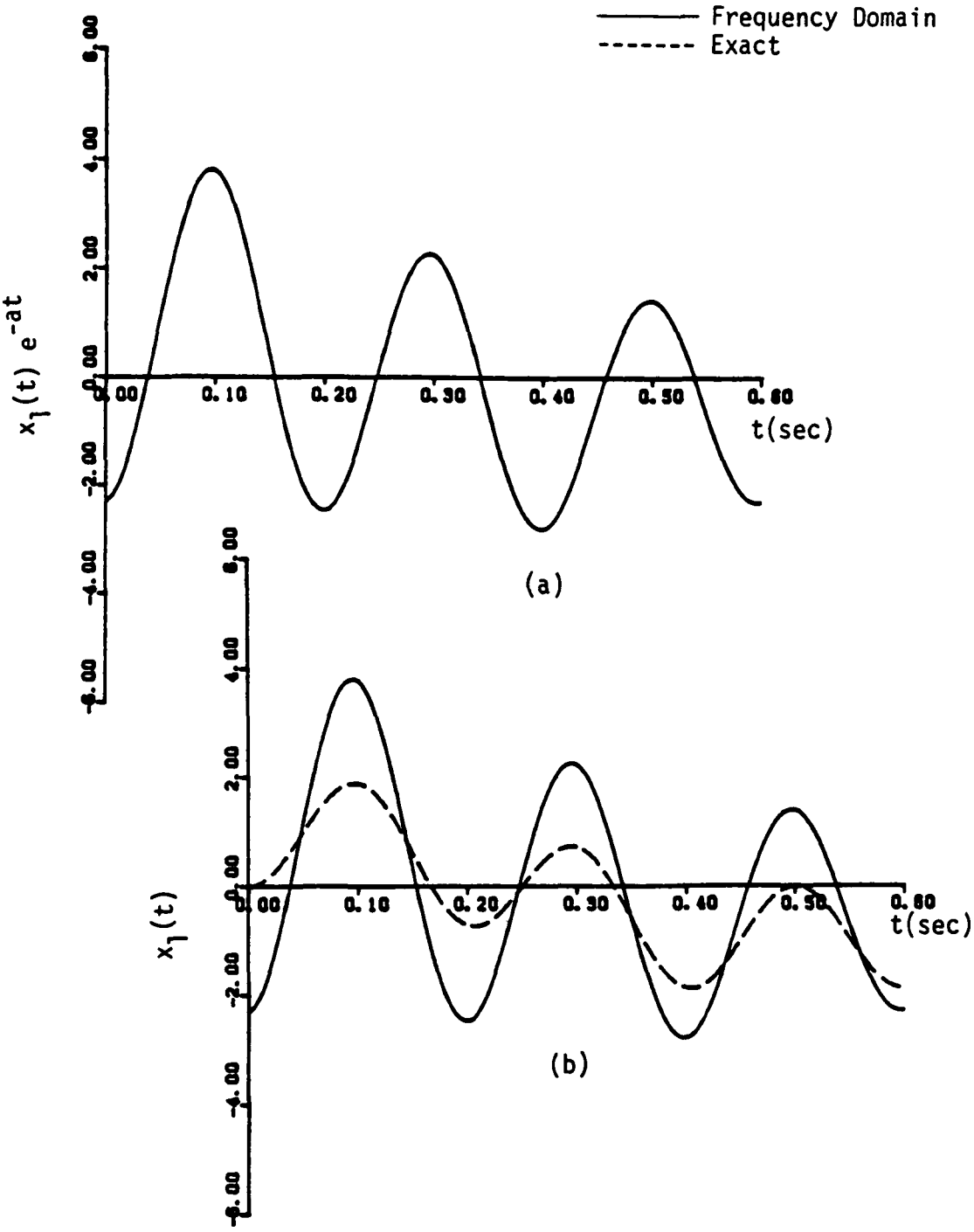

Figure 7.6 (a) Exponentially-windowed response and (b) the response with the window removed (a = 1.0).

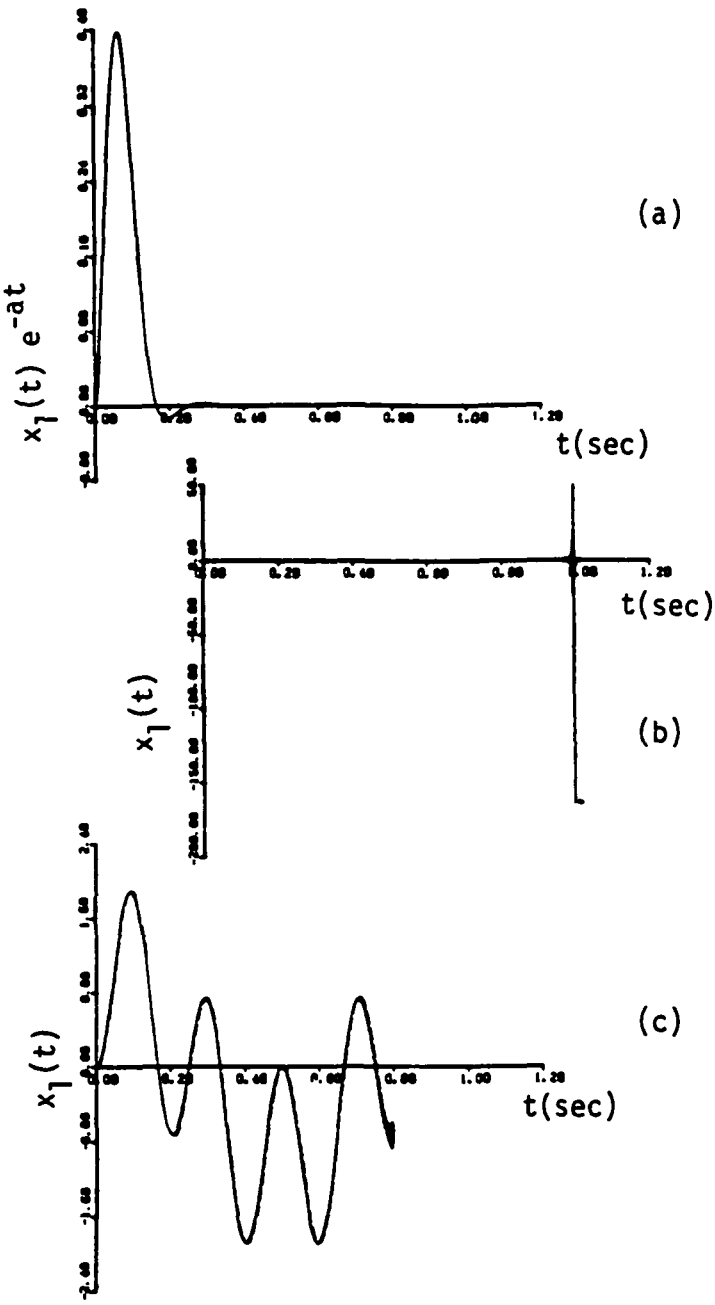

Figure 7.7 (a) Exponentially-windowed response, (b) the response with the window removed, and (c) the first 0.8 seconds of the response (a = 30.0).

domain solutions in Figure 7.6b is not good, as the frequency-domain solution is time-aliased.

There is, however, a problem with selecting a convergence factor which is too large, and which causes the windowed response to be 'effectively zero' too early in the window. In order to demonstrate the problem, let

$$a = 30.0$$

and let the response window be 1.0 seconds long. Thus,

$$T_o = 1.0 \quad .$$

The exponentially-windowed response shown in Figure 7.7a reveals that the windowed response is 'effectively zero' at $t = 0.2$ seconds. Therefore, it is clear that the solution will not be time-aliased. However, an examination of Figure 7.7b reveals that the frequency-domain solution of the response is not stable near the end of the window. Figure 7.7c shows the response for the first 0.8 seconds of the window, and it can be seen that the response prior to the region of instability compares well with the exact solution.

Example 2

This example will demonstrate the substructure coupling procedures discussed in Chapter 4. The superstructure to be used in this example is an 18 degree-of-freedom beam clamped at each end.

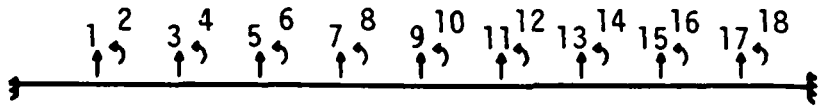

Substructure 0

The beam will be analyzed using the two substructures,

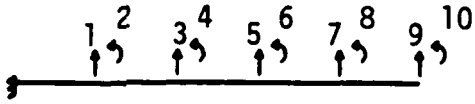

Substructure 1

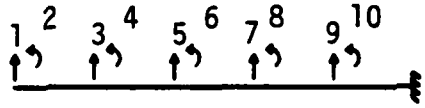

Substructure 2

The structure will be loaded at the translational degree of freedom of the interface with the following load,

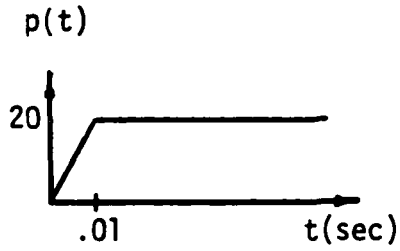

Assuming the response is desired at only the loaded degree of freedom, the relevant set may be determined by taking the union of the following sets:

Interface DOF	9,10
Loaded DOF	9
Response DOF	9

Therefore, the relevant set consists of

Relevant DOF	9,10

Note that even though the response is not desired at system degree-of-freedom 10, it must be determined, since interface degrees of freedom are required to be in the relevant set.

Assuming the first 0.1 second of the response is desired,

$$T_o = 0.1 \text{ sec}$$

and the maximum value of the convergence factor is

$$a = 46.05$$

An examination of a typical transfer function for the system shown in Figure 7.8 reveals that the transfer function is not 'effectively zero,' even at frequencies greater than 2000 Hz. However, Figure 7.9 reveals that the exponentially-windowed force spectra is 'effectively zero' by 200 Hz, therefore,

$$f_c = 200 \text{ Hz}$$

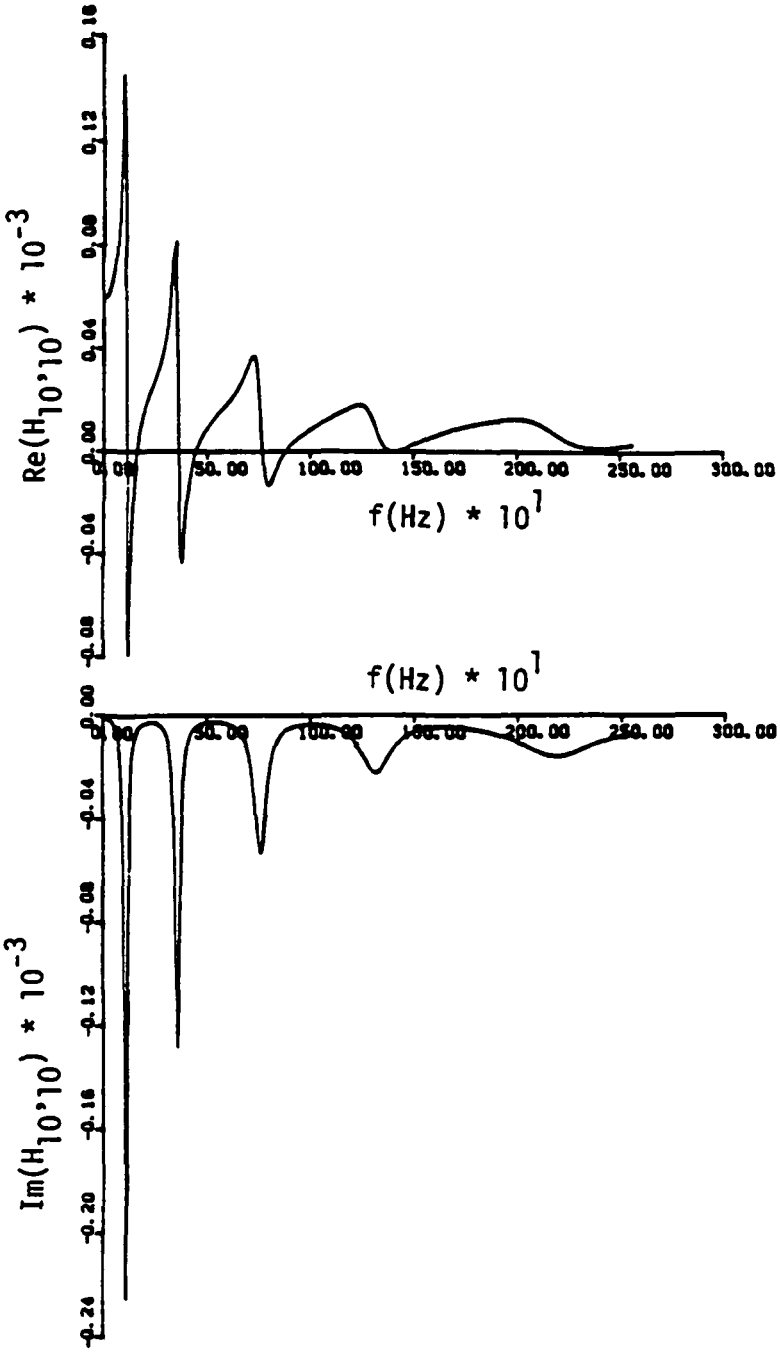

Figure 7.8 System transfer function (a = 46.05).

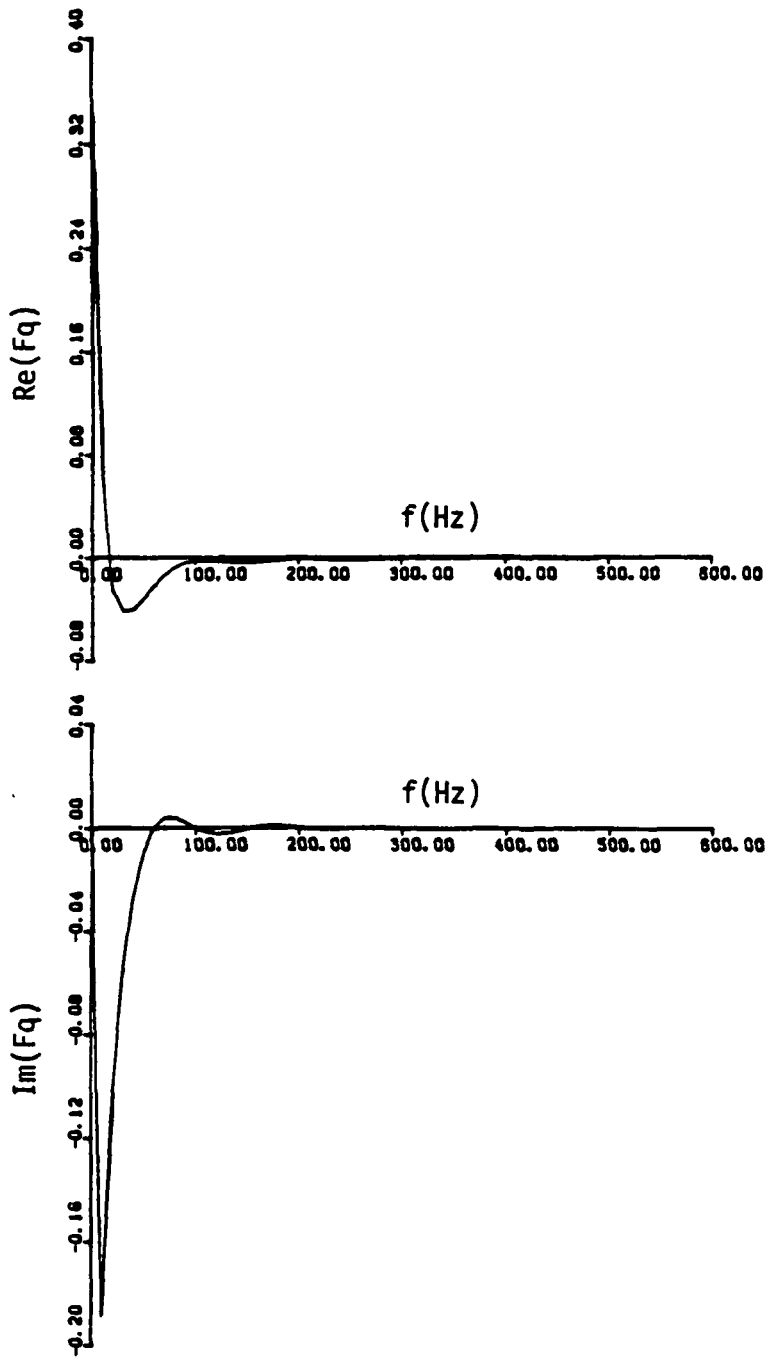

Figure 7.9 Exponentially-windowed force spectra (0-500 Hz).

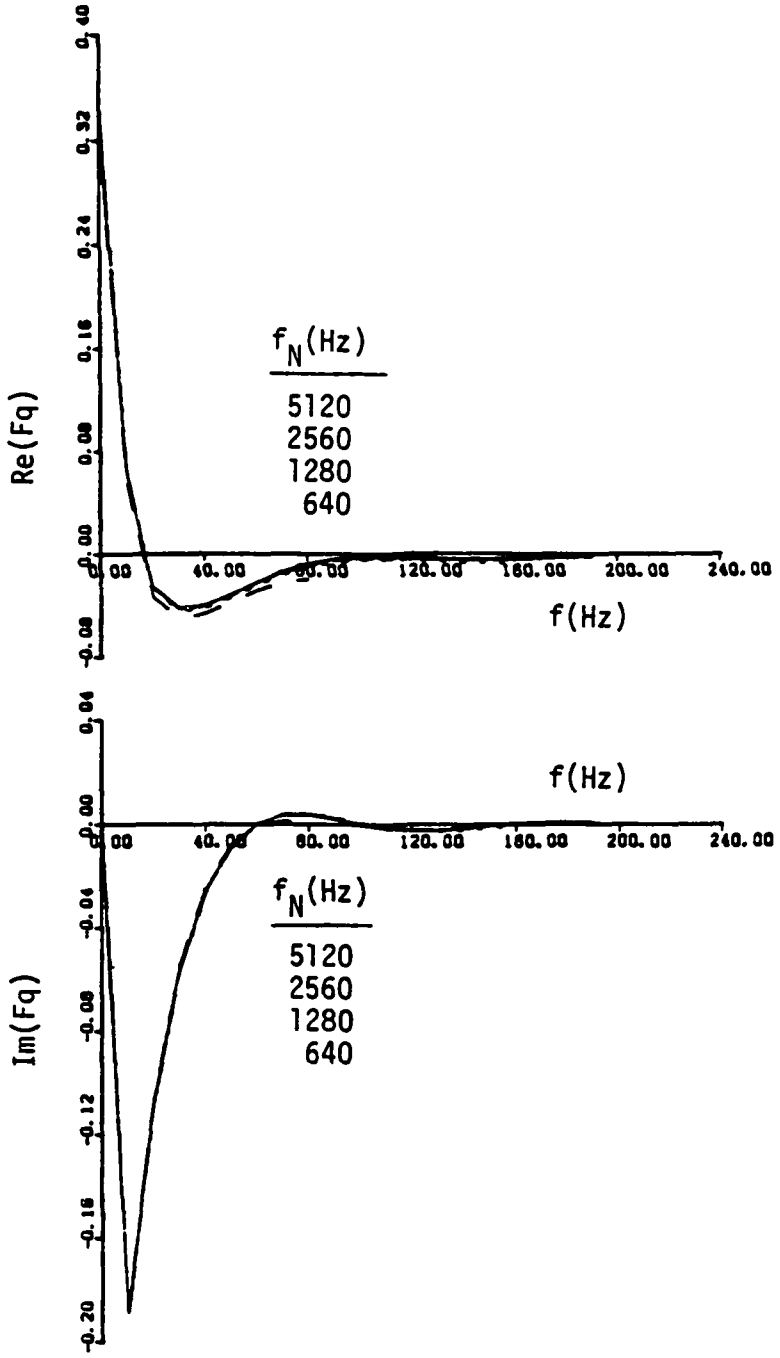

Figure 7.10 Exponentially-windowed force spectra for various Nyquist frequencies (0-200 Hz).

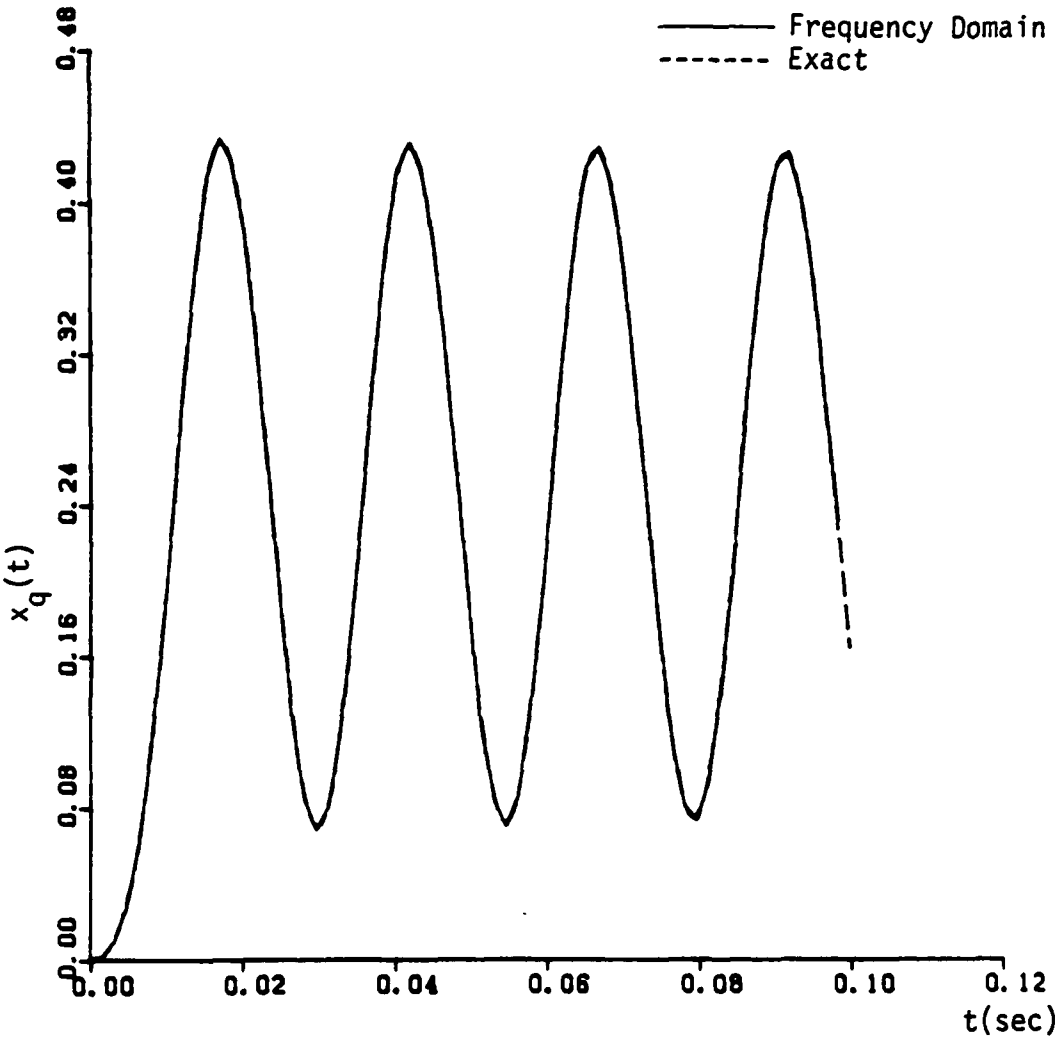

Figure 7.11 System response to a step-to-ramp input.

An examination of Figure 7.10 reveals that the spectra have nearly converged for a Nyquist frequency of 2560 Hz. Thus, let

$$f_N = 2560 \text{ Hz}$$

This Nyquist frequency may now be used to obtain the remaining sampling parameters and the exponentially-windowed force spectrum.

An eigensolution may now be performed on each of the substructures to obtain the generalized mass, stiffness and modal matrices, which are required for the modal formation of the dynamic stiffness transfer matrix. The frequency loop and the inverse transformation outlined in Figure 4.3 may now be executed to obtain the time-domain response of the desired system degree of freedom.

The response obtained using the frequency-domain substructuring procedure described above is plotted in Figure 7.11 along with an accepted time-domain solution. The solutions compare very well, and thus the substructuring technique has been verified.

Example 3

This example will demonstrate the recovery of superstructure natural frequencies from frequency-domain substructure models. The superstructure chosen for the example is the six degree-of-freedom mass spring oscillator,

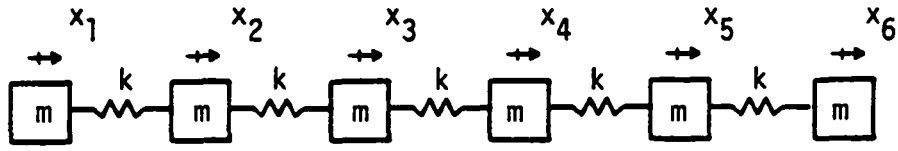

Substructure 0

m = 1.0 k = 1.0

which will be analyzed using the two substructures,

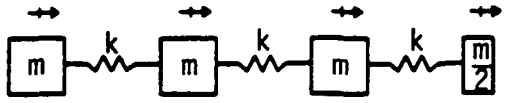

Substructure 1

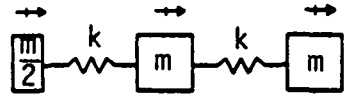

Substructure 2

The two substructures are joined by one common interface degree of freedom. Thus,

$$p_I^o = 1$$

In order to determine the superstructure natural frequencies, the fixed interface natural frequencies of each substructure must be obtained. They have been determined and tabulated below.

Substructure Natural Frequencies
(rads/sec)

Substructure 1	Substructure 2
0.4450	0.6180
1.2470	1.6180
1.8019	

The search parameters will be chosen such that the natural frequencies will be calculated to within 0.001 rads/sec and the search range will be from 0-100 rads/sec. Thus,

$$TOL = 0.001 \text{ (rads/sec)}$$

$$\omega_{min} = 0.000 \text{ (rads/sec)}$$

$$\omega_{max} = 100.0 \text{ (rads/sec)}$$

The system natural frequencies may now be obtained using the above information and the dynamic stiffness transfer matrices of the substructures, as directed by the outline in Figure 5.3.

After an average of 10 polynomial evaluations (i.e. 10 times through the bisection loop) per natural frequency, the system natural frequencies were determined to be

Substructure 0 Natural Frequencies
(rads/sec)

0.000
0.518
1.000
1.414
1.733
1.933

The characteristic equation of the reduced system is shown in Figure 7.12. The figure also illustrates how each of the Sturm sequence indices changes as a function of frequency. Note that the value of $\bar{S}$ is never greater than one, since p_I^0 is equal to one. From the figure, it can be seen that S is the sum of $\bar{S}$ and S_{SB}^0, and that the r^{th} natural frequency is located at the frequency where S changes from $r-1$ to r.

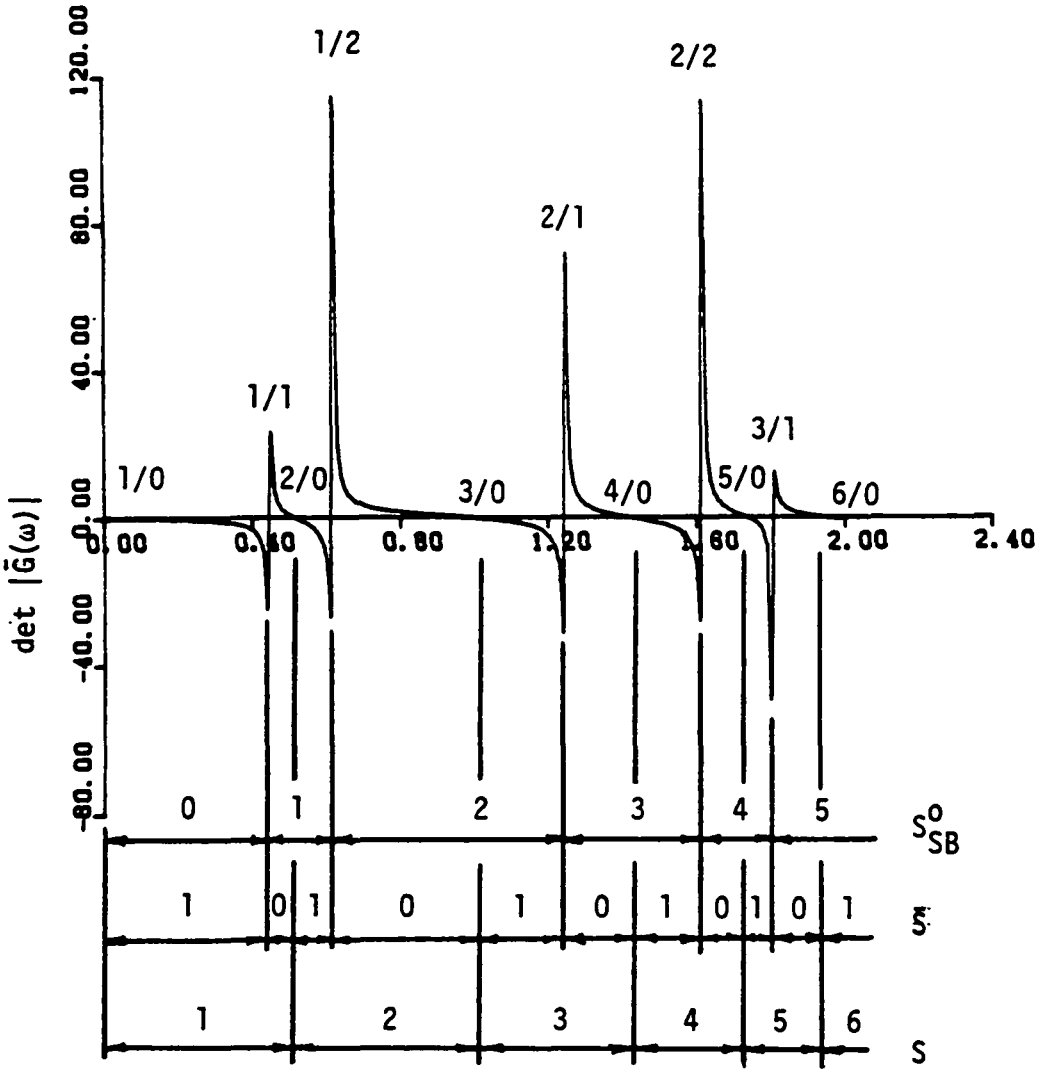

Note: r/j = r^{th} natural frequency of the j^{th} substructure

Figure 7.12 Characteristic equation and Stürm sequence indices of a 6 degree of freedom system.

Example 4

This final example is included to demonstrate the applicability of Eqs. (6.8) and (6.9) for determining the damped natural frequencies of the damped mass-spring oscillator below.

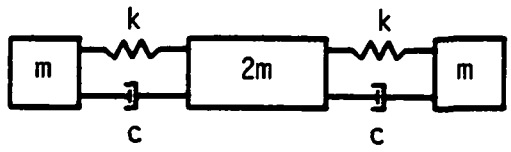

Substructure 0

$m = 1.0 \qquad k = 1.0 \qquad c = 0.05$

The natural frequencies will be determined using the two substructures,

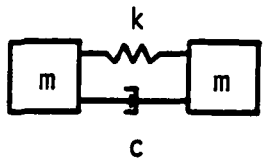

Substructure 1

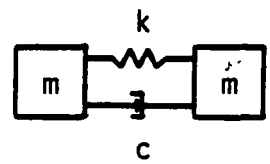

Substructure 2

which have one common interface degree of freedom, and thus

$$p_I^o = 1$$

The fixed-interface natural frequency of both substructure 1 and substructure 2 is $(-0.05 + j1.413)$, since each of the substructures are identical. In order to use the bilinear search procedure described in Chapter 6, the range of the imaginary part of the natural frequencies has been chosen to be 0-2 rads/sec, and the tolerance as 0.00001 rads/sec.

After an average of 60 polynomial evaluations per root, the damped natural frequencies of the superstructure were determined to be

Superstructure Damped Natural Frequencies

$$-.0095 + j0.618$$
$$-.5000 + j1.413$$
$$-.6545 + j1.617$$

These natural frequencies match precisely the damped natural frequencies obtained from an exact solution of the equations of motion describing the system.

As noted in Chapter 6, a single example does not explicitly prove that Eqs. (6.8) and (6.9) are valid for all systems; however, it does demonstrate their applicability in obtaining the damped natural frequencies of at least one particular problem.

Chapter 8

CONCLUSIONS

8.1 Solving the Response Problem

Frequency-domain analysis has been found to be an efficient method for finding the frequency response of a structure and has been used by structural analysts for many years. The research completed for this thesis has also found it to be a suitable method for determining the transient response of systems subjected to a wide variety of loads. However, since a large number of calculations are performed within the discrete frequency loop, the method loses its computational efficiency if the load must be represented by a large number of discrete frequencies.

It has also been discovered that substructure coupling in the frequency domain works particularly well for analyzing structural systems with a small number of interface and loaded degrees of freedom. A system with these restrictions will have relatively small matrices within the frequency loop, which increases the efficiency of the frequency-domain procedure.

The ability to describe large complex substructures by the dynamic stiffness and loads at only the interface degrees of freedom makes substructure coupling in the frequency domain very attractive for structural modification problems as well.

8.2 Determining the Natural Frequencies

In an attempt to determine the generality of frequency-domain analysis, it was discovered that substructure coupling in the frequency domain can lead to an efficient method of obtaining natural frequencies of undamped structures. The efficiency, however, decreases as the number of interface degrees of freedom increases.

It has also been found that the damped natural frequencies of a system may be determined using frequency-domain techniques. However, the algorithm used to determine these natural frequencies has not been proven explicitly.

8.3 Directions for Future Research

Over the past two decades substructure coupling in the time domain has played an important role in the analysis and design of structures. In order for substructure coupling in the frequency domain to play a similar role, it will be necessary for the following items to be investigated:

- A more in-depth study on the effects of using a convergence factor in transient response analyses.
- A solution procedure for analyzing response to random excitation.
- The effects which modal truncation at the substructure level has on the system response and natural frequencies.

- A proof of Eqs. (6.8) and (6.9), which were used to determine the damped natural frequencies of the superstructure.

With these topics clarified, substructure coupling in the frequency domain could play an important role in the design and analysis of future structural systems.

APPENDIX A. TRANSFORMING THE EQUATIONS OF MOTION

A.1 Unilateral Fourier Integral Transform

The unilateral Fourier transform pair chosen for this thesis may be written as

$$Y(\omega) = \int_0^\infty y(t)\, e^{-j\omega t}\, dt \qquad (A.1)$$

$$y(t) = \frac{1}{2\pi} \int_{-\infty}^{\infty} Y(\omega)\, e^{j\omega t}\, d\omega \qquad (A.2)$$

In order for the unilateral Fourier integral transform of $y(t)$ to exist, and for $y(t)$ to be recoverable from its transform, the following conditions must be satisfied:

a) In every finite interval, $y(t)$ must be bounded and have a finite number of maxima and minima, and a finite number of discontinuities.

b) The integral

$$\lim_{A\to\infty} \int_0^A |y(t)|\, dt \equiv \int_0^\infty |y(t)|\, dt \qquad (A.3)$$

converges (i.e. the integral approaches some finite limit as A approaches infinity).

Since both the system excitation and response will be transformed to the frequency domain, each must satisfy the conditions

stated above. The first condition will be satisfied for any stable system subjected to a physically-realizable excitation. The second condition may be satisfied by many functions. However, this discussion will assume the excitation and response are identically zero beyond some finite value of t. This assumption will ensure convergence of the integral given by Eq. (A.3) (Ref. LePage).

Therefore, with the transformability conditions satisfied, the system equation of motion, Eq. (2.1), may now be transformed to the frequency domain using Eq. (A.1).

$$\int_0^\infty \left[[m]\{\ddot{x}\} + [c]\{\dot{x}\} + [k]\{x\}\right] e^{-j\omega t}\, dt = \int_0^\infty \{f(t)\}\, e^{-j\omega t}\, dt \tag{A.4}$$

The integration of the first two terms by parts yields

$$\int_0^\infty [m]\{\ddot{x}\}\, e^{-j\omega t}\, dt = [m]\{\dot{x}\}\, e^{-j\omega t}\Big|_0^\infty + j\omega[m]\{x\}\, e^{-j\omega t}\Big|_0^\infty - \omega^2[m]\int_0^\infty \{x\}\, e^{-j\omega t}\, dt \tag{A.5}$$

$$\int_0^\infty [c]\{\dot{x}\}\, e^{-j\omega t}\, dt = [c]\{x\}\, e^{-j\omega t}\Big|_0^\infty + j\omega[c]\int_0^\infty \{x\}\, e^{-j\omega t}\, dt \tag{A.6}$$

and combining terms yields

$$\left[-\omega^2[m] + j\omega[c] + [k]\right] \int_0^\infty \{x\}\, e^{-j\omega t}\, dt$$

$$= \int_0^\infty \{f(t)\}\, e^{-j\omega t}\, dt \; - \; [m]\{\dot{x}\}\, e^{-j\omega t}\,\Big|_0^\infty \qquad (A.7)$$

$$- \left[\, j\omega[m] + [c]\right]\{x\}\, e^{-j\omega t}\,\Big|_0^\infty$$

The evaluation of the last two terms on the right hand side of Eq. (A.7) at the lower limit is accomplished by using the identity

$$e^{-j\omega t}\,\Big|_{t=0} = e^0 = 1 \qquad (A.8)$$

Although $e^{-j\omega t}$ is not defined at $t = \infty$, it is known that $|e^{-j\omega\infty}| \leq 1$, and therefore the terms may be evaluated at their upper limit by recalling the assumption of finite-duration response. That is to say,

$$\{x\}\big|_{t=\infty} = \{0\} \qquad (A.9)$$

$$\{\dot{x}\}\big|_{t=\infty} = \{0\} \qquad (A.10)$$

Therefore, Eq. (A.7) may be simplified and written

$$\left[-\omega^2[m] + j\omega[c] + [k]\right]\{X(\omega)\} = \{\tilde{F}(\omega)\} + [m]\{\dot{x}_0\} \qquad (A.11)$$

$$+ \left[\, j\omega[m] + [c]\right]\{x_0\}$$

where

$$X(\omega) = \int_0^\infty \{x\}\, e^{-j\omega t}\, dt \tag{A.12}$$

$$\tilde{F}(\omega) = \int_0^\infty \{f(t)\}\, e^{-j\omega t}\, dt \tag{A.13}$$

$$\{\dot{x}_0\} = \{\dot{x}(t=0)\} \tag{A.14}$$

$$\{x_0\} = \{x(t=0)\} \tag{A.15}$$

Eq. (A.11) represents the system equations of motion in the frequency domain, and is subject to the restriction that the excitation be nonperiodic and of finite duration. It is also restricted to those systems which are damped, in order that the response will also be of finite duration.

A.2 Unilateral Fourier Integral Transform with Convergence Functions

The unilateral Fourier integral transform pair with convergence functions may be written as

$$Y(\omega) = \int_0^\infty \hat{y}(t)\, e^{-j\omega t}\, dt \tag{A.16}$$

$$y(t) = \frac{e^{at}}{2\pi} \int_{-\infty}^{\infty} Y(\omega)\, e^{j\omega t}\, d\omega \tag{A.17}$$

where

$$\hat{y}(t) = y(t)\, e^{-at} \tag{A.18}$$

In order for the unilateral Fourier integral transform of $\hat{y}(t)$ to exist, and for $y(t)$ to be recoverable from its transform, the following conditions must be satisfied.

a) In every finite interval, $\hat{y}(t)$ must be bounded and have a finite number of maxima and minima, and a finite number of discontinuities.

b) The integral

$$\int_0^\infty |y(t)|e^{-at}\,dt \tag{A.19}$$

converges.

As in Appendix A.1, both the system excitation and response must satisfy the conditions stated above, and the first condition is satisfied for any stable system subjected to a physically-realizable excitation. However, the second condition will not restrict the class of problems which can be worked, so long as a value of the convergence factor, a , may be found which is greater than zero and causes Eq. (A.19) to converge.

The equation of motion, Eq. (2.1), may now be transformed using Eq. (A.16). Thus,

$$\int_0^\infty \left[[m]\{\ddot{x}\} + [c]\{\dot{x}\} + [k]\{x\}\right] e^{-at}\, e^{-j\omega t}\,dt = \int_0^\infty \{f(t)\}\, e^{-at}\, e^{-j\omega t}\,dt \tag{A.20}$$

and simplifying yields

$$\int_0^\infty \left[[m]\{\ddot{x}\} + [c]\{\dot{x}\} + [k]\{x\} \right] e^{-st}\, dt = \int_0^\infty \{f(t)\}\ e^{-st}\, dt \qquad (A.21)$$

where the complex frequency variable, s, is given by

$$s = a + j\omega \qquad (A.22)$$

The integration by parts of the first two terms yields

$$\left[[m]s^2 + [c]s + [k] \right] \int_0^\infty \{x\}\, e^{-st}\, dt \qquad (A.23)$$

$$= \int_0^\infty \{f(t)\}\, e^{-st}\, dt - [m]\{\dot{x}\}\, e^{-st}\Big|_0^\infty - \left[[m]s + [c] \right] \{x\}\, e^{-st}\Big|_0^\infty$$

Now, the last two terms on the right hand side of Eq. (A.23) may be evaluated at the lower limit using the identity

$$e^{-st}\Big|_{t=0} = e^{\circ} = 1 \qquad (A.24)$$

and, at the upper limit, since $a > 0$

$$e^{-st}\Big|_{t=\infty} = e^{-\infty} = 0 \qquad (A.25)$$

Therefore, Eq. (A.23) may be simplified and written

$$\left[[m]\, s^2 + [c]\, s + [k] \right] \{X(s)\} \qquad (A.26)$$

$$= \{\tilde{F}(s)\} + [m]\, \{\dot{x}_o\} + \left[[m]\, s + [c] \right]\ \{x_o\}$$

where

$$\{X(s)\} = \int_0^\infty \{x\}\ e^{-st}\ dt \qquad (A.27)$$

$$\{\tilde{F}(s)\} = \int_0^\infty \{f(t)\}\ e^{-st}\ dt \qquad (A.28)$$

$$\{\dot{x}_0\} = \{\dot{x}\ (t=0)\} \qquad (A.29)$$

$$\{x_0\} = \{x\ (t=0)\} \qquad (A.30)$$

Equation (A.26) represents the system equations of motion in the complex frequency domain. The only restriction on the system, is that a convergence factor exists such that Eq. (A.19) converges.

A.3 Complex Fourier Series

Assume that the system described by Eq. (2.1) is subjected to a periodic excitation which may be represented by

$$\{f(t)\} = \{\tilde{F}\}\ e^{j\Omega t} \qquad (A.31)$$

Now, assume the response will be represented in a similar form

$$\{x(t)\} = \{X\}\ e^{j\Omega t} \qquad (A.32)$$

Equation (A.31), along with Eq. (A.32) and its derivatives may now be substituted into Eq. (2.1) to yield

$$\left[-\Omega^2\ [m] + j\Omega\ [c] + [k]\right] \{X\}\ e^{j\Omega t} = \{\tilde{F}\}\ e^{j\Omega t} \qquad (A.33)$$

or in a simplified form as

$$[G(\Omega)]\ \{X\} = \{\tilde{F}\} \tag{A.34}$$

Equation (A.34) may now be solved for $\{X\}$, which is then substituted into Eq. (A.32) to obtain the steady-state response of the system to the periodic excitation $\{f(t)\}$

$$\{x(t)\} = [G(\Omega)]^{-1}\ \{\tilde{F}\}\ e^{j\Omega t} \tag{A.35}$$

For physically-realizable periodic excitations which are composed of more than one frequency, the excitation can be represented by the complex Fourier series transform pair

$$\{f(t)\} = \frac{1}{T_1} \sum_{k=-\infty}^{\infty} \{\tilde{F}(\omega_k)\}\ e^{j\omega_k t} \tag{A.36}$$

$$\{\tilde{F}(\omega_k)\} = \int_{\tau}^{\tau+T_1} \{f(t)\}\ e^{-j\omega_k t}\ dt \tag{A.37}$$

where

$$\omega_k = k\left(\frac{2\pi}{T_1}\right) \tag{A.38}$$

and T_1 is the fundamental period of the excitation.

For linear systems, the principal of superposition may be invoked to obtain the total response

$$\{x(t)\} = \frac{1}{T_1} \sum_{k=-\infty}^{\infty} [G(\omega_k)]^{-1}\ \{\tilde{F}(\omega_k)\}\ e^{j\omega_k t} \tag{A.39}$$

where

$$[G(\omega_k)] = -\omega_k^2 [m] + j\omega_k [c] + [k] \tag{A.40}$$

In order that a frequency-domain equation may be written in a form similar to those in Appendices A.1 and A.2, Eq. (A.39) will be transformed to the frequency domain and written

$$\left[-\omega_k^2 [m] + j\omega_k [c] + [k]\right] \{X(\omega_k)\} = \{\tilde{F}(\omega_k)\} \tag{A.41}$$

$$k = -\infty, \ldots, \infty$$

where

$$\{X(\omega_k)\} = \int_{\tau}^{\tau+T_1} \{x(t)\} \, e^{-j\omega_k t} \, dt \tag{A.42}$$

and $\{\tilde{F}(\omega_k)\}$ is given in Eq. (A.37).

Therefore, Eq. (A.41) represents the equation of motion in the frequency domain which describes the steady-state response of a system subjected to periodic excitation.

APPENDIX B. DISCRETE FOURIER TRANSFORM

In the discussion of the Discrete Fourier Transform (DFT) and the Fast Fourier Transform (FFT) in Chapter 3, the following notation, parameter relationships and terminology are often utilized.

Notation

f_s - sampling frequency

f_N - Nyquist frequency

f_o - frequency resolution

T_o - length of the time record

T - time resolution

K - number of discrete samples

Relationships

$$f_N = \frac{1}{2T} \tag{B.1}$$

$$f_s = 2f_N \tag{B.2}$$

$$T_o = \frac{1}{f_o} \tag{B.3}$$

$$T = \frac{T_o}{K} \tag{B.4}$$

Terminology

Frequency-Domain Aliasing - Frequency-domain aliasing occurs when the sampling frequency is less than twice the highest frequency contained

in the continuous function being transformed. It is characterized by the energy of the frequencies which are greater than f_N, folding back into the lower frequencies. This increased energy in the lower frequencies of the force spectrum will cause the response spectrum to also have higher energies in the low frequencies.

Time-Domain Aliasing - Time-domain aliasing occurs when the frequency resolution is not fine enough to allow the inverse transform of a frequency function to be effectively zero by the end of the time record T_0. It is characterized by the nonzero part of the function extending beyond T_0, adding back into the function at the beginning of the time record.

Leakage - Leakage occurs when the time record does not contain an integer number of fundamental periods of a periodic function. It is characterized by energy from the fundamental frequency showing up in frequencies adjacent to the fundamental frequency.

LIST OF REFERENCES

1. NASTRAN Theoretical Manual, NASA SP-221(03).

2. G.J. DeSalvo and J.A. Swanson, ANSYS Engineering Analysis System User's Manual, Swanson Analysis Systems, Inc., Houston, PA (1982).

3. H.P. Geering, "New Methods in Substructuring," AIAA/ASME/ASCE/AHS 21st Structures, Structural Dynamics and Materials Conference, Seattle, Washington, May 12-14, 1980.

4. R.J. Thornhill and C.C. Smith, Fourier and Spectral Analysis - A Short Course (1980).

5. D. Poelaert, "Dynamic Analysis of a Nonrigid Spacecraft - An Eigenvalue Approach," ESA Journal, V. 1, n. 3, pp. 269-281.

6. F.W. Williams and W.H. Wittrick, "An Automatic Computational Procedure for Calculating Natural Frequencies of Skeletal Structures," Int. J. Mech. Sci., V. 12, 781-791 (1970).

7. A.K. Chopra and P. Chakrabarti, "Earthquake Analysis of Concrete Gravity Dams Including Dam-Water-Foundation Rock Interaction," Earthquake Engineering and Structural Dynamics, V. 9, 363-383 (1981).

8. K.R. Payne, An Impedance Technique for Determining Low-Frequency Payload Environments, NASA CR-3143, Martin Marietta Corp., Denver, CO (1979).

9. W.R. LePage, Complex Variables and the Laplace Transform for Engineers, Dover Publications, Inc., New York, NY (1961).

10. E.O. Brigham, The Fast Fourier Transform, Prentice-Hall, Englewood Cliffs, NJ (1974).

11. C.T. Chen, One Dimensional Digital Signal Processing, Marcel Dekker, Inc., New York, NY (1979).

12. J.W. Cooley and J.W. Tukey, "An Algorithm for Machine Calculation of Complex Fourier Series," Math Computation, V. 19, 297-301.

13. Caughey, T.L., "Classical Normal Modes in Damped Linear Dynamic Systems," Journal of Applied Mechanics, V. 27, 269-271 (1960).

14. R.R. Craig, Structural Dynamics, John Wiley and Sons, New York, NY (1981).

15. R.W. Clough and J. Penzien, Dynamics of Structures, McGraw-Hill Book Co., New York, NY (1975).

16. A.J. Salmonte, "Consideration of the Residual Contribution in Modal Analysis," Earthquake Engineering and Structural Dynamics, V. 10, 295-304 (1982).

17. J.H. Wilkinson, The Algebraic Eigenvalue Problem, Clarendon Press, Oxford (1965).

18. K.J. Bathe and E.L. Wilson, Numerical Methods in Finite Element Analysis, Prentice-Hall, Englewood Cliffs, NJ (1976).